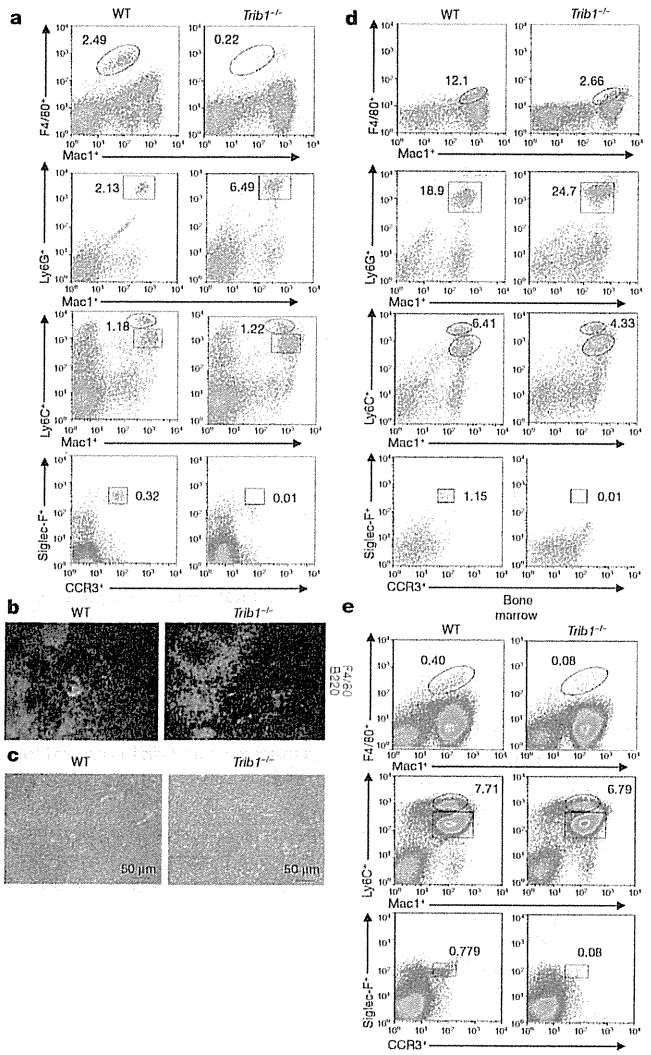


**Figure 1 | Lack of tissue-resident M2-like macrophages and eosinophils in *Trib1*-deficient mice.** **a**, Flow cytometric analyses of splenocytes. The expression levels of F4/80$^+$ and Mac1$^+$ tissue-resident M2-like macrophages in splenocytes are shown (top). The proportions of inflammatory monocytes and neutrophils (middle) and eosinophils (bottom) in splenocytes are also shown. Similar results were obtained in eight independent experiments. **b**, Wild-type (WT) and *Trib1*$^{-/-}$ spleen sections were stained for F4/80 (red) and B220 (green). **c**, Images of Perl's Prussian blue staining for ferric iron in the spleens of wild-type and *Trib1*$^{-/-}$ mice. Scale bars, 50 μm. **d**, Flow cytometric analysis of cell populations in the blood. The percentages of F4/80$^+$ and Mac1$^+$ cells in the blood are shown. **e**, Flow cytometric analysis of bone marrow. The percentages of F4/80$^+$ and Mac1$^+$ tissue-resident M2-like macrophages in the bone marrow are shown (top). The proportions of inflammatory monocytes and neutrophils (middle) and eosinophils (bottom) in the bone marrow are also shown. Similar results were obtained in three independent experiments (**b**–**e**).

differentiation of bone marrow myeloid cells. Proportions of CMP and CLP as well as GMP were comparable between wild-type and *Trib1*$^{-/-}$ mice (see Supplementary Fig. 11 for definitions). Furthermore, the expression pattern of transcriptional factors, which are involved in myeloid cell differentiation, in GMP and MDP was also comparable between wild-type and *Trib1*$^{-/-}$ mice (Supplementary Fig. 12), suggesting that Trib1 controls myeloid cell differentiation downstream of GMP.

Retroviral expression of full-length Trib1 in *Trib1*$^{-/-}$ bone marrow cells resulted in a marked increase in aggregated and small macrophage colonies and eosinophil colonies, but decreased granulocyte/

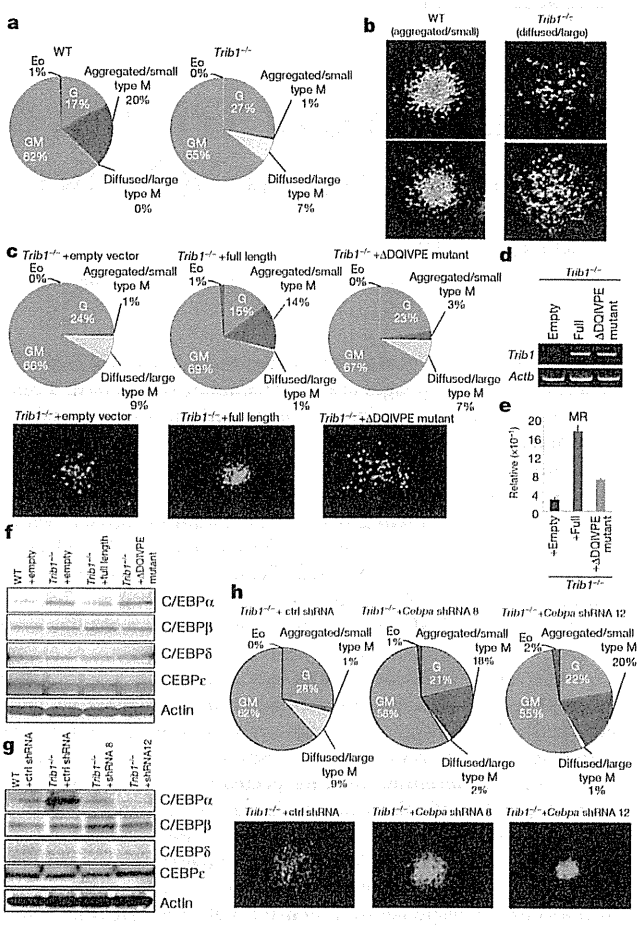


**Figure 2 | Trib1 controls macrophage, eosinophil and neutrophil differentiation via the ubiquitin-binding domain.** **a**, **b**, Bone marrow cells were subjected to colony-forming assays. Each colony was counted depending on the morphology (**a**), and images of the cell types of macrophage colonies are shown (**b**). Eo, eosinophil colonies; G, granulocyte/neutrophil colonies; GM, granulocyte/macrophage colonies; M, macrophage colonies. **c**–**e**, Role of the COP1-binding site in macrophage differentiation. Bone marrow cells lacking *Trib1* were infected with retroviruses expressing empty vector, full-length Trib1 (mTrib1) or Trib1(ΔDQIVPE) mutant. Colony-forming assays were performed in retrovirus-infected (GFP$^+$) cells. Images of the retrovirus-infected (GFP$^+$) cell types of macrophage colonies are shown in **c**. **d**, Semi-quantitative PCR analyses were performed to measure the expression of *Trib1* in empty vector, full-length Trib1 (full length) or mutant Trib1(ΔDQIVPE) in macrophage colonies. **e**, Quantitative PCR analyses were performed for MR expression in macrophage colonies expressing empty vector, Trib1 (full length) or mutant Trib1(ΔDQIVPE). Error bars indicate s.d. of duplicates. Similar results were obtained in three independent experiments (**a**–**e**). **f**, Immunoblot analyses of various C/EBP family molecules. Lineage-negative fractions from wild-type, *Trib1*$^{-/-}$ cells, *Trib1*$^{-/-}$ cells expressing full-length and *Trib1*$^{-/-}$ cells expressing mutant Trib1(ΔDQIVPE) were analysed by western blotting. **g**, **h**, Role of C/EBPα in macrophage differentiation. Bone marrow cells lacking *Trib1* were infected with retroviruses expressing empty vector, *Cebpa* shRNA 8 or *Cebpa* shRNA 12. Immunoblot analyses of various C/EBP family molecules. Lineage-negative fractions from wild-type, *Trib1*$^{-/-}$ cells and *Trib1*$^{-/-}$ cells expressing *Cebpa* shRNA 8 or *Cebpa* shRNA 12 were analysed by western blotting (**g**). Colony-forming assays were performed in infected (GFP$^+$) cells, and images of the retrovirus-infected (GFP$^+$) cell types of macrophage colonies are shown (**h**). Similar results were obtained in two independent experiments (**f**–**h**).

neutrophil colonies (Fig. 2c, d and Supplementary Fig. 13). In contrast, expression of Trib1 lacking the COP1-binding site (Trib1(ΔDQIVPE) mutant) in *Trib1*$^{-/-}$ bone marrow cells failed to restore the differentiation defects. Moreover, expression of full-length Trib1, but not of

Trib1(ΔDQIVPE) mutant, restored expression of M2 macrophage marker genes such as *MR* (Fig. 2e). Next, we investigated the expression of potential target proteins of the Trib1–COP1 axis in *Trib1*$^{-/-}$ bone marrow cells. Among the transcription factors, C/EBP family members are important for determining the balance between granulopoiesis and monopoiesis[18]. We found that expression of C/EBPα, but not other transcriptional factors involved in myeloid cell differentiation, was increased in lineage-negative bone marrow cells and macrophage colonies lacking Trib1 (Fig. 2f and Supplementary Fig. 14). The expression of full-length Trib1 in *Trib1*$^{-/-}$ bone marrow cells suppressed the level of C/EBPα expression (Fig. 2f). To address whether increased expression of C/EBPα is involved in aberrant myeloid cell differentiation under Trib1 deficiency, we genetically inhibited *Cebpa* in *Trib1*$^{-/-}$ bone marrow cells using short hairpin RNAs (shRNAs) (Supplementary Fig. 15). The decreased C/EBPα protein expression in *Trib1*$^{-/-}$ bone marrow cells was similar to levels of

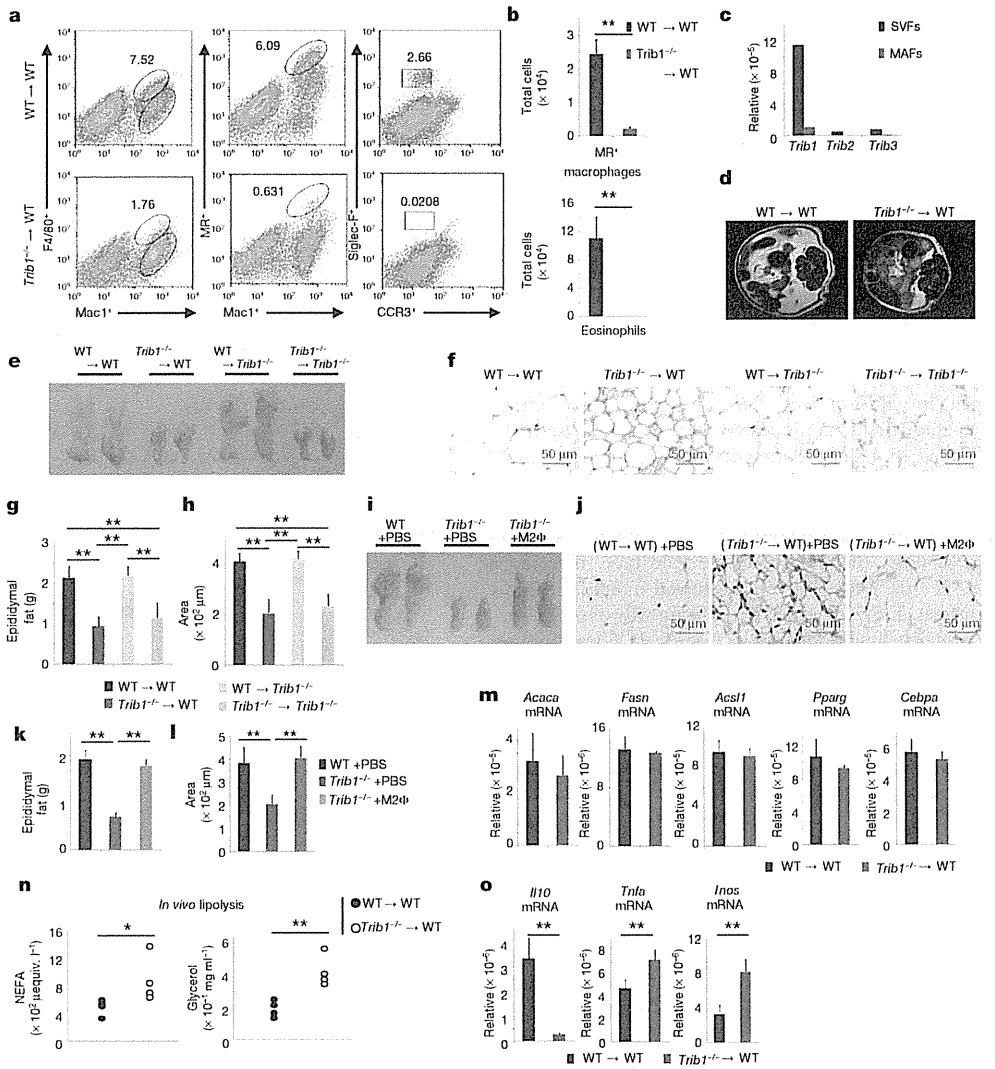


**Figure 3 | Impact of Trib1 deficiency on lipodystrophy.** **a**, **b**, Flow cytometric analyses of haematopoietic cells in adipose tissue. The expression levels of F4/80$^{+}$ and Mac1$^{+}$ or MR$^{+}$ and Mac1$^{+}$ tissue-resident M2 macrophages in adipose tissue (left and centre) and Siglec-F$^{+}$ and CCR3$^{+}$ eosinophils (right) are shown. The total numbers of MR$^{+}$ macrophages and eosinophils in adipose tissues from wild-type and *Trib1*$^{-/-}$ chimaeric mice fed a normal diet are shown (**b**). Error bars indicate s.d. of duplicates. Similar results were obtained in three independent experiments. **c**, Expression levels of *Trib1*, *Trib2* and *Trib3* in SVFs and MAFs, assessed by quantitative PCR. Similar results were obtained in two independent experiments. **d**, The epididymal adipose tissues from wild-type and *Trib1*$^{-/-}$ chimaeric mice fed a normal diet were analysed by magnetic resonance imaging (MRI). **e**, Images of the epididymal adipose tissues from each indicated chimaeric mice fed a normal diet are shown. **f**, Haematoxylin and eosin-stained images of paraffin-embedded epididymal adipose tissue sections from each indicated chimaeric mice fed a normal diet. Scale bars, 50 μm. **g**, **h**, The total epididymal fat weight was measured (**g**) and each area of adipocytes was measured (**h**) in each indicated chimaeric mouse. Error bars indicate s.d. of duplicates. **i**, Images of the epididymal adipose tissues from each indicated chimaeric mice fed a normal diet are shown. **j**, Haematoxylin-and-eosin-stained images of paraffin-embedded epididymal adipose tissue sections from each indicated chimaeric mice fed a normal diet. Scale bars, 50 μm. **k**, **l**, The total epididymal fat weight (**k**) and each area of adipocytes were measured (**l**) in each indicated chimaeric mouse. Error bars indicate s.d. of duplicates. **m**, Total RNA was prepared from wild-type and *Trib1*$^{-/-}$ chimaeric mice fed a normal diet. The expression levels of mRNAs encoding the indicated proteins were determined by quantitative PCR. Error bars indicate s.d. of duplicates. Similar results were obtained in three independent experiments (**e**–**m**). **n**, Lipolysis assays in wild-type and *Trib1*$^{-/-}$ mice fed a normal diet. The serum glycerol and NEFA levels were measured *in vivo*. Similar results were obtained in two independent experiments. **o**, Total RNA was prepared from wild-type and *Trib1*$^{-/-}$ chimaeric mice fed a normal diet. The expression levels of mRNAs encoding the indicated proteins were determined by quantitative PCR. Error bars indicate s.d. of duplicates. Similar results were obtained in three independent experiments. Statistical significance in **b**, **g**, **h**, **k**, **l**, **n**, **o** was determined using the Student's *t*-test. $^{*}P < 0.05$; $^{**}P < 0.01$.

wild-type cells (Fig. 2g). Repression of *Cebpa* resulted in an increase in the aggregated and small macrophage colonies and eosinophil colonies, but a decrease in granulocyte/neutrophil colonies (Fig. 2h). Taken together, these data demonstrate that Trib1 regulates myeloid cell differentiation by altering the expression of C/EBPα in a COP1-dependent manner.

Recent genome-wide association studies revealed that genetic variants in the loci corresponding to *TRIB1* are associated with increased plasma lipoprotein concentrations, a high risk of ischaemic heart disease and myocardial infarction in humans[8–10]. These studies prompted us to investigate the role of Trib1 in the adipose tissue and liver of mice. Because we did not observe histological changes in the liver in the absence of Trib1 in mice fed normal chow (Supplementary Fig. 16), we next examined the adipose tissues. Consistent with observations in other organs, $MR^+F4/80^+$ adipose-tissue-resident M2-like macrophages were severely decreased in the stromal vascular fraction (SVF) derived from *Trib1*$^{-/-}$ epididymal adipose tissues compared with wild-type mice (Supplementary Fig. 17). Mice lacking Trib1 in haematopoietic cells also showed a reduced number of M2-like macrophages and lacked eosinophils in epididymal adipose tissues (Fig. 3a, b), and *Trib1* mRNA was rarely expressed in the normal mature adipocyte fraction (MAF) (Fig. 3c), indicating that the defect is intrinsic to haematopoietic cells. In contrast, $CD11c^+Mac1^+$ M1 macrophages were hardly present in wild-type and *Trib1*$^{-/-}$ adipose tissues from mice fed a normal chow diet (Supplementary Fig. 17). Unexpectedly, MRI analyses revealed that Trib1 deficiency in haematopoietic cells severely reduced the abdominal adipose tissues (Fig. 3d). The epididymal adipose tissues and size of each epididymal adipocyte were significantly smaller in mice lacking Trib1 in all tissues as well as in haematopoietic cells only, than in littermate wild-type mice fed a normal diet (Fig. 3e–h). Thus, the mice showed a lipodystrophic phenotype. In contrast, *Trib1*$^{-/-}$ mice harbouring wild-type haematopoietic cells did not develop lipodystrophy (Fig. 3e, f). These findings demonstrate that Trib1 deficiency in haematopoietic cells is responsible for development of this pathophysiology. To investigate whether loss of M2-like macrophages is responsible for the development of lipodystrophy, we supplemented *Trib1*$^{-/-}$ mice with these macrophages (Supplementary Fig. 18). After 3 weeks, the epididymal adipose tissues and the size of each adipocyte from *Trib1*$^{-/-}$ mice reconstituted with these macrophages were significantly larger than in PBS-treated *Trib1*$^{-/-}$ mice (Fig. 3i–l). Collectively, these data indicate that lack of M2-like macrophages, caused by Trib1 deficiency, is important for the development of the lipodystrophic phenotype.

Next, we examined the mechanisms of the lipodystrophy caused by Trib1 deficiency in haematopoietic cells. Adipose tissues are maintained by balance between lipogenesis and lipolysis. The mRNA levels of genes involved in adipocyte differentiation and lipogenesis were comparable between wild-type and *Trib1*$^{-/-}$ bone marrow chimaeric mice (Fig. 3m and Supplementary Fig. 19; see Methods). In contrast, the serum levels of non-esterified fatty acids (NEFAs) and glycerol were significantly elevated in *Trib1*$^{-/-}$ bone marrow chimaeric mice (Fig. 3n), indicative of enhanced lipolysis caused by Trib1 deficiency. Cytokines produced by macrophages contribute to adipose tissue inflammation and lipolysis. Expression of IL-10 was severely reduced in epididymal adipose tissues lacking Trib1 in haematopoietic cells. In contrast, *Tnf* and *Inos* mRNA expression were elevated in adipose tissues from *Trib1*$^{-/-}$ bone marrow chimaeric mice (Fig. 3o). Because several reports indicated that IL-10 has a central role in repressing lipolysis in adipocytes in addition to having anti-inflammatory effects[19–21], it is possible that M2-like macrophages are important for maintaining adipose tissues, at least in part, through the production of IL-10. However, the contribution of additional molecules produced by the macrophages may also be critical for amelioration of lipodystrophy.

Lipodystrophy is often associated with metabolic abnormalities. Although significant differences in levels of the parameters such as serum glucose, cholesterol, triglyceride and insulin were not detected between wild-type and *Trib1*$^{-/-}$ bone marrow chimaeric mice fed a normal diet, the feeding of mice with a high-fat diet (HFD) led to much higher elevations of these parameters in the serum of *Trib1*$^{-/-}$ bone marrow chimaeric mice (Fig. 4a). Mice lacking Trib1 throughout the whole body and in haematopoietic cells also developed glucose intolerance and insulin resistance on a HFD (Fig. 4b, c and Supplementary Fig. 20). In contrast, body weight did not differ significantly between wild-type and *Trib1*$^{-/-}$ bone marrow chimaeric mice fed a HFD (Supplementary Fig. 21). Whereas numbers of M1-type macrophages increased in both wild-type and *Trib1*$^{-/-}$ bone marrow chimaeric mice as well as mice lacking Trib1 in the whole body fed a HFD,

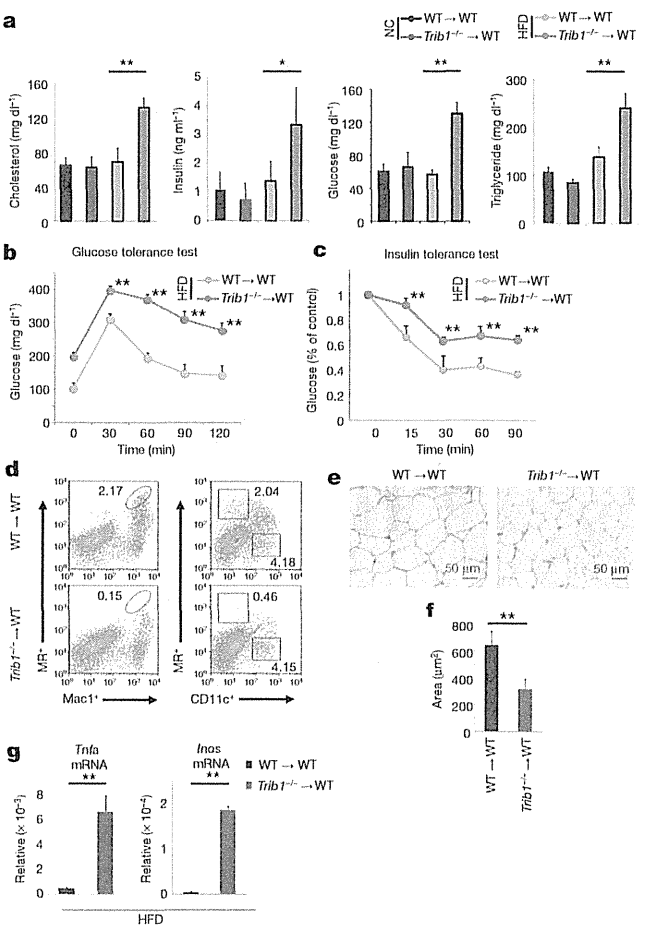


**Figure 4 | Mice lacking Trib1 in haematopoietic cells develop exacerbated metabolic disorders on a high-fat diet.** **a**, Serum samples were obtained from bone-marrow-transferred wild-type and *Trib1*$^{-/-}$ littermates fed normal chow (NC) or a high-fat diet (HFD). The concentrations of cholesterol, insulin, glucose and triglyceride were measured. Error bars indicate s.d. of duplicates. **b**, **c**, Fasting male bone-marrow-transferred wild-type and *Trib1*$^{-/-}$ littermates fed a HFD were challenged with intraperitoneal glucose (**b**) or insulin (**c**), and blood was sampled for glucose analyses at the indicated times. Data are mean s.d. of 5 samples. **d**, Flow cytometric analyses of haematopoietic cells from adipose tissues in wild-type and *Trib1*$^{-/-}$ mice fed a HFD. The expression levels of $MR^+$ and $Mac1^+$ tissue-resident macrophages are shown (left). The $MR^+$ and $CD11c^+$ macrophages in adipose tissue are also shown (right). **e**, **f**, Haematoxylin-and-eosin-stained images of paraffin-embedded epididymal adipose tissue sections are shown (**e**), and each area of adipocytes was measured (**f**). Scale bars, 50 μm. **g**, Total RNA was prepared from wild-type and *Trib1*$^{-/-}$ chimaeric mice fed a HFD. Error bars indicate s.d. of duplicates. The expression levels of mRNAs encoding the indicated genes were determined by quantitative PCR. Error bars indicate s.d. of duplicates. Statistical significance in **a**–**c**, **f**, **g** was determined using the Student's *t*-test. $*P < 0.05$; $**P < 0.01$.

M2-like macrophages were severely decreased in the absence of Trib1 (Fig. 4d and Supplementary Fig. 22). *Trib1*$^{-/-}$ chimaeric mice had smaller adipocytes on a HFD (Fig. 4e, f). Notably, *Tnf* and *Inos* mRNA were markedly augmented in *Trib1*$^{-/-}$ chimaeric mice (Fig. 4g). Taken together, these findings suggest that *Trib1*$^{-/-}$ bone marrow chimaeric mice develop metabolic disorders on a HFD through impaired lipid buffering caused by lipodystrophy.

Although we previously showed that Trib1 regulates C/EBPβ expression in thioglycollate-elicited macrophages[11], we found that M2-like macrophages were present in *Cebpb*$^{-/-}$ mice (data not shown). Thus, Trib1 seems to control different target proteins for degradation depending on the cell types and their differentiation stages. We previously showed that Jmjd3 is essential for M2-like macrophage differentiation in response to chitin administration and helminth infection[22,23]. However, Jmjd3 deficiency did not show any defect in tissue-resident M2-like macrophage generation (Supplementary Fig. 23). Reciprocally, Trib1 deficiency did not alter the activation of M2-like macrophages to chitin administration (Supplementary Fig. 24). It can be assumed that macrophage subtypes are more complex *in vivo*, although the precise classification of M2-type macrophages *in vivo* is yet to be clarified.

Chronic low-grade inflammation in adipose tissues is thought to have a central role in the exacerbation of metabolic disorders[24,25]. M1-type macrophages infiltrate into obese adipose tissues via MCP1, where they are activated in part by saturated fatty acids and cause low-grade inflammation by producing proinflammatory cytokines[26,27]. However, tissue-resident M2-like macrophages, which differentiate depending on the presence of Trib1 in the bone marrow, are subsequently activated in adipose tissues and the liver in response to IL-4 and IL-13 produced from eosinophils by a PPAR-γ- and PPAR-δ-dependent mechanism, respectively[21,28–30]. Further studies are required to clarify how tissue-resident M2-like macrophages maintain adipose tissue homeostasis. Trib1 was also essential for the development of eosinophils, nevertheless, we believe that Trib1 maintains adipose tissues by controlling M2-like macrophages, as supplementation of wild-type macrophages alone could rescue the lipodystrophy observed in *Trib1*$^{-/-}$ mice.

Mutations in TRIB1 have been implicated in metabolic disorders of humans. It is tempting to speculate that TRIB1 functions in a similar manner in humans and that other pathophysiologies, such as tumour progression, angiogenesis or tissue remodelling, are affected by these tissue-resident M2-like macrophages.

## METHODS SUMMARY

**Mice, reagents, cells and plasmids.** Full details are provided in the Methods.

**Colony-forming assay.** Bone marrow cells ($4 \times 10^4$) were seeded on 3.5-cm dishes and cultured for 7 days with Methocult (no. 3534; Stem Cell Technologies) containing SCF, IL-6 and IL-3 in the presence of 20 ng ml$^{-1}$ M-CSF. The numbers of GFP-positive cells were counted for colony-forming assays or collected for real-time (q)PCR and western blotting.

**Full Methods** and any associated references are available in the online version of the paper.

**Received 19 March 2012; accepted 22 January 2013.**
**Published online 20 March 2013.**

1. Martinez, F. O., Helming, L. & Gordon, S. Alternative activation of macrophages: an immunologic functional perspective. *Annu. Rev. Immunol.* **27,** 451–483 (2009).
2. Biswas, S. K. & Mantovani, A. Macrophage plasticity and interaction with lymphocyte subsets: cancer as a paradigm. *Nature Immunol.* **11,** 889–896 (2010).
3. Mantovani, A. & Sica, A. Macrophages, innate immunity and cancer: balance, tolerance, and diversity. *Curr. Opin. Immunol.* **22,** 231–237 (2010).
4. Takeuchi, O. & Akira, S. Pattern recognition receptors and inflammation. *Cell* **140,** 805–820 (2010).
5. Medzhitov, R. Origin and physiological roles of inflammation. *Nature* **454,** 428–435 (2008).
6. Sica, A. & Mantovani, A. Macrophage plasticity and polarization: *in vivo* veritas. *J. Clin. Invest.* **122,** 787–795 (2012).
7. Yokoyama, T. *et al.* Trib1 links the MEK1/ERK pathway in myeloid leukemogenesis. *Blood* **116,** 2768–2775 (2010).
8. Varbo, A., Benn, M., Tybjaerg-Hansen, A., Grande, P. & Nordestgaard, B. G. TRIB1 and GCKR polymorphisms, lipid levels, and risk of ischemic heart disease in the general population. *Arterioscler. Thromb. Vasc. Biol.* **31,** 451–457 (2011).
9. Aung, L. H. *et al.* Association of the TRIB1 tribbles homolog 1 gene rs17321515 A>G polymorphism and serum lipid levels in the Mulao and Han populations. *Lipids Health Dis.* **10,** 230 (2011).
10. Chambers, J. C. *et al.* Genome-wide association study identifies loci influencing concentrations of liver enzymes in plasma. *Nature Genet.* **43,** 1131–1138 (2011).
11. Yamamoto, M. *et al.* Enhanced TLR-mediated NF-IL6 dependent gene expression by Trib1 deficiency. *J. Exp. Med.* **204,** 2233–2239 (2007).
12. Jin, G. *et al.* Trib1 and Evi1 cooperate with Hoxa and Meis1 in myeloid leukemogenesis. *Blood* **109,** 3998–4005 (2007).
13. Keeshan, K. *et al.* Tribbles homolog 2 inactivates C/EBPα and causes acute myelogenous leukemia. *Cancer Cell* **10,** 401–411 (2006).
14. Du, K., Herzig, S., Kulkarni, R. N. & Montminy, M. TRB3: A *tribbles* homolog that inhibits Akt/PKB activation by insulin in liver. *Science* **300,** 1574–1577 (2003).
15. Okamoto, H. *et al.* Genetic deletion of Trb3, the mammalian *Drosophila* tribbles homolog, displays normal hepatic insulin signaling and glucose homeostasis. *Diabetes* **56,** 1350–1356 (2007).
16. Kohyama, M. *et al.* Role for Spi-C in the development of red pulp macrophages and splenic iron homeostasis. *Nature* **457,** 318–321 (2009).
17. De Domenico, I., McVey Ward, D. & Kaplan, J. Regulation of iron acquisition and storage: consequences for iron-linked disorders. *Nature Rev. Mol. Cell Biol.* **9,** 72–81 (2008).
18. Hong, S., Skaist, A. M., Wheelan, S. J. & Friedman, A. D. AP-1 protein induction during monopoiesis favors C/EBP: AP-1 heterodimers over C/EBP homodimerization and stimulates FosB transcription. *J. Leukoc. Biol.* **90,** 643–651 (2011).
19. Odegaard, J. I. & Chawla, A. Alternative macrophage activation and metabolism. *Annu. Rev. Pathol.* **6,** 275–297 (2011).
20. Lumeng, C. N., Bodzin, J. L. & Saltiel, A. R. Obesity induces a phenotypic switch in adipose tissue macrophage polarization. *J. Clin. Invest.* **117,** 175–184 (2007).
21. Odegaard, J. I. *et al.* Macrophage-specific PPARγ controls alternative activation and improves insulin resistance. *Nature* **447,** 1116–1120 (2007).
22. Reese, T. A. *et al.* Chitin induces accumulation in tissue of innate immune cells associated with allergy. *Nature* **447,** 92–96 (2007).
23. Satoh, T. *et al.* The Jmjd3-Irf4 axis regulates M2 macrophage polarization and host responses against helminth infection. *Nature Immunol.* **11,** 936–944 (2010).
24. Chawla, A., Nguyen, K. D. & Goh, Y. P. Macrophage-mediated inflammation in metabolic disease. *Nature Rev. Immunol.* **11,** 738–749 (2011).
25. Gregor, M. F. & Hotamisligil, G. S. Inflammatory mechanisms in obesity. *Annu. Rev. Immunol.* **29,** 415–445 (2011).
26. Hotamisligil, G. S. Inflammation and metabolic disorders. *Nature* **444,** 860–867 (2006).
27. Wellen, K. E. & Hotamisligil, G. S. Obesity-induced inflammatory changes in adipose tissue. *J. Clin. Invest.* **112,** 1785–1788 (2003).
28. Wu, D. *et al.* Eosinophils sustain adipose alternatively activated macrophages associated with glucose homeostasis. *Science* **332,** 243–247 (2011).
29. Odegaard, J. I. *et al.* Alternative M2 activation of Kupffer cells by PPARδ ameliorates obesity-induced insulin resistance. *Cell Metab.* **7,** 496–507 (2008).
30. Ricardo-Gonzalez, R. R. *et al.* IL-4/STAT6 immune axis regulates peripheral nutrient metabolism and insulin sensitivity. *Proc. Natl Acad. Sci. USA* **107,** 22617–22622 (2010).

**Supplementary Information** is available in the online version of the paper.

**Acknowledgements** We thank I. Shimomura and Y. Miyata for providing us with the key protocols for the metabolic experiments; T. Kitamura for providing the PlatE cells; M. Higa, H. Tanaka, N. Miyamoto, K. Miura, D. Ori, T. Uehata and K. Kuniyoshi for assistance with the experiments; and T. Kawai, S. Uematsu, T. Saitoh and Y. Kumagai for discussions. We also thank E. Kamada and M. Kageyama for secretarial assistance, and N. Umano, Y. Matsumoto and M. Kumagai for technical assistance. This work was supported by the Special Coordination Funds of the Japanese Ministry of Education, Culture, Sports, Science and Technology, and the Ministry of Health, Labour and Welfare in Japan, the Japan Society for the Promotion of Science through the Funding Program for World-Leading Innovative R&D on Science and Technology (FIRST Program).

**Author Contributions** T.S. designed and performed the experiments and wrote the manuscript. H.K., H.N. and N. Takakura performed the colony-forming assays. M.Y. generated the *Trib1*$^{-/-}$, *Trib2*$^{-/-}$ and *Trib3*$^{-/-}$ mice. N. Takemura helped with experiments. K.N. performed microarray analysis. Y.Y. performed the MRI experiments. E.M. performed the histological analyses. O.T. and S.A. designed experiments and wrote the manuscript. S.A. supervised the project.

**Author Information** Data have been deposited in the GEO under accession number GSE43563. Reprints and permissions information is available at www.nature.com/reprints. The authors declare no competing financial interests. Readers are welcome to comment on the online version of the paper. Correspondence and requests for materials should be addressed to S.A. (sakira@biken.osaka-u.ac.jp).

## METHODS

**Mice, cells and reagents.** *Trib1*$^{-/-}$ mice were generated as described previously[11]. Antibodies for flow cytometry were purchased from commercial sources as follows: anti-F4/80-FITC (BM8; BioLegend); anti-Mac1-PerCP Cy5.5 (M1/70; BD Biosciences); anti-Ly6C-FITC (AL-21; BD Biosciences); anti-Siglec-F-PE (E50-2446; BD Biosciences); anti-CCR3-APC (83103; BD Biosciences); anti-MR-Alexa 488 (MR5D3; BioLegend); and anti-CD11c-Brilliant bright (N418; BioLegend). Antibodies and reagents for histochemical analysis were purchased from commercial sources as follows: biotinylated anti-F4/80 (eBioscience), anti-MOMA-1 (Abcam), Alexa 488-conjugated anti-B220 (BD Pharmingen) and streptavidin-Alexa594 (Invitrogen). Antibodies for western blotting were purchased as follows: anti-C/EBPα (no. 2295; Cell Signaling Technology); anti-C/EBPβ (no. E298; Millipore); anti-C/EBPδ (no. 2318; CST); anti-C/EBPε (no. sc-158; Santa Cruz Biotechnology); and anti-actin (no. sc-1615; Santa Cruz Biotechnology). The probes for quantitative PCR were purchased from Lifescience Japan.

**Generation of *Trib2*$^{-/-}$ and *Trib3*$^{-/-}$ mice.** The *Trib2* and *Trib3* genes were isolated from genomic DNA extracted from embryonic stem (ES) cells (GSI-I) by PCR. The targeting vectors were constructed by replacing a 2-kilobase (kb) fragment encoding the *Trib2* open reading frame (exon 2) and replacing a 2.5-kb fragment encoding the *Trib3* open reading frame (exons 2–3) with a neomycin-resistance gene cassette (*neo*), and inserting herpes simplex virus thymidine kinase (HSV-TK) driven by the PGK promoter into the genomic fragment for negative selection. After each targeting vector was transfected into ES cells, G418 and ganciclovir double-resistant colonies were selected and screened by PCR, and recombination was further confirmed by Southern blotting. The homologous recombinant clones were individually microinjected into blastocysts derived from C57BL/6 mice and then transferred to pseudopregnant females. Mating of chimaeric male mice with C57BL/6 female mice resulted in the transmission of each mutant allele to the germ line. The resulting *Trib2*$^{+/-}$ and *Trib3*$^{+/-}$ mice were interbred to generate *Trib2*$^{-/-}$ *and Trib3*$^{-/-}$ mice, respectively. All animal experiments were performed with approval from the Animal Research Committee of the Research Institute for Microbial Diseases (Osaka University).

**Construction of expression plasmids and shRNA vectors.** *Trib1* and *Cebpa* cDNAs were obtained by PCR from a mouse cDNA library. Full-length or mutated *Trib1* cDNAs were cloned into the pLZR-cmv-ires-GFP vector for retrovirus production. For shRNA experiments, the following oligonucleotides were used to target mouse C/EBPα: cebpa-8 dn, 5′-gatccGTCGTATGTATTATATCTATA TTCAAGAGATATAGATATAATACATACGACTTTTTTACGCGTg-3′ and cebpa-8 up, 5′-aattcACGCGTAAAAAAGTCGTATGTATTATATCTATATC TCTTGAATATAGATATAATACATACGACg-3′; cebpa-12 dn, 5′-gatccATCC GATATCAACACTTGTATTTCAAGAGAATACAAGTGTTGATATCGGATT TTTTTACGCGTg-3′ and cebpa-12 up, 5′-aattcACGCGTAAAAAAATCCGA TATCAACACTTGTATTCTCTTGAAATACAAGTGTTGATATCGGATg-3′. The oligonucleotides were annealed and ligated with the RNAi-ready pSIREN-RetroQ-zsGreen vector (Takara). Lowercase letters indicate the site of restriction enzyme.

**Colony-forming assay.** Bone marrow cells ($4 \times 10^4$) were seeded on 3.5-cm dishes and cultured for 7 days with Methocult (no. 3534; Stem Cell Technologies) containing SCF, IL-6 and IL-3 in the presence of 20 ng ml$^{-1}$ M-CSF. The numbers of GFP-positive cells were counted for colony-forming assays or collected for real-time (q)PCR and western blotting.

**Assessment of glucose, insulin and NEFA levels and glucose and insulin sensitivity *in vivo*.** Serum insulin levels were determined by ELISA (Morinaga Institute of Biological Science Inc.). Serum glucose, NEFA and cholesterol levels were measured with enzymatic kits (WAKO Chemicals). Intraperitoneal glucose tolerance tests were performed on 16 h fasted mice injected intraperitoneally with D-glucose (1.5 mg g$^{-1}$ body weight). Serum glucose levels were measured immediately before and 30, 60, 90 and 120 min after the D-glucose injection. Intraperitoneal insulin tolerance tests were performed on 4 h fasted mice injected intraperitoneally with insulin (1 mU g$^{-1}$ body weight). Serum glucose levels were measured immediately before and 15, 30, 60 and 90 min after the insulin injection.

**Lipolysis assay.** *In vivo* lipolysis assays were performed on 4 h fasted mice. Blood was collected from orbital veins, and the serum glycerol and NEFA concentrations were measured.

**Quantitative PCR analysis.** Total RNA was isolated using Trizol (Invitrogen) and subjected to reverse transcription with ReverTra Ace (Toyobo) according to the manufacturer's instructions. For quantitative PCR, cDNA fragments were amplified using real-time PCR Master Mix (Toyobo). Fluorescence from the TaqMan probe for each cytokine was detected using a 7500 Real-time PCR System (Applied Biosystems). To determine the relative induction of each cytokine mRNA in response to various stimuli, the mRNA expression level of each gene was normalized to the 18S rRNA expression level. The experiments were repeated at least twice.

Assay ID numbers are: *Arg1*, Mm00475988_m1, *Ym1*, Mm00657889_mH, *Fizz1*, Mm00445109_m1, *MR*, Mm00485148_m1; *Trib1*, Mm00454875_m1; *Trib2*, Mm0045 4876_m1; *Trib3*, Mm00454879_m1; *Acaca*, Mm01304277_m1; *Fasn*, Mm00662319_m1; *Acsl1*, Mm00484217_m1; *PParg*, Mm01184322_m1; *Cebpa*, Mm00514283_s1; *Cebpb*, Mm00843434_s1; *Cebpd*, Mm00786711_s1; *Il10*, Mm00439614_m1; *Tnfa*, Mm99999068_m1; *Inos*, Mm00440485_m1.

**Immunoblot analysis.** Bone marrow cells were collected and red blood cells were lysed using red blood cell lysis buffer (Invitrogen). After two washes with MACS buffer, lineage-negative cells were collected by MACS sorting using anti-CD3, anti-CD19, anti-B220, anti-Ter119, anti-Gr1, anti-DX5, anti-Mac1 and anti-CD11c MACS beads (Miltenyi Biotec). The lineage-negative cells were lysed with lysis buffer (20 mM Tris-HCl, pH 7.5, 150 mM NaCl, 1 mM EDTA, 1% NP40) containing Complete Protease Inhibitor Cocktail (Roche). The cell lysates were separated by standard SDS–PAGE and analysed by immunoblotting. Antibodies against the following proteins were used: C/EBPα, C/EBPβ, C/EBPδ, C/EBPε and actin. The Luminata Forte Western HRP Substrate (Millipore) was used for the development of positive signals.

**Flow cytometry.** Cell suspensions were prepared by sieving and gentle pipetting. After washing with ice-cold FACS buffer (0.5% BSA and 2 mM EDTA in PBS, pH 7.2), the cells were incubated with antibodies for 15 min and washed twice with FACS buffer. Data were acquired using a FACSCalibur flow cytometer (BD), and analysed by FlowJo software (Tree Star).

**Retroviral preparation.** Retroviruses were produced using PlatE packaging cells or transfected with various plasmids. Bone marrow cells were transduced with the retroviral supernatants (supplemented with polybrene (Millipore)) twice. After the second transduction, the cells were washed twice and re-suspended in RPMI medium.

**Magnetic resonance imaging (MRI).** An 11.7 T MRI scanner (AVANCE-II 500 WB; Bruker BioSpin) was used to acquire *in vivo* mouse images. Mice were anaesthetized with 1.0–1.5% isoflurane during the MRI procedures. We used a $T_2$-weighted imaging sequence (RARE) with the following parameters: field of view, 2.5 × 2.5 cm; matrix size, 256 × 256; slice thickness, 0.5 mm; repetition time, 5,000 ms; echo time, 25.2 ms; average, 4; scan time, 5 min.

**Histochemical analysis.** Frozen 6-μm tissue sections were fixed in 4% paraformaldehyde and blocked with 5% BSA (Invitrogen). For Perl's Prussian blue staining, tissues were fixed with 4% paraformaldehyde in phosphate buffer (pH 7.0), embedded in paraffin and stained with Perl's Prussian blue.

**Generation of bone-marrow-transferred chimaeric mice.** Bone marrow cells were prepared from wild-type and *Trib1*$^{-/-}$ mice, and intravenously injected into lethally irradiated CD45.1 C57BL/6 mice, wild-type and *Trib1*$^{-/-}$ mice. The chimaeric mice were administered neomycin (Sigma) and polymyxin B (Sigma) in their drinking water for 8 weeks. The mice were analysed for at least 12 weeks after reconstitution. More than 90% of splenocytes from the chimaeric mice were CD45.2$^+$.

**Mouse SVF and MAF isolation.** Epididymal fat pads from male mice fed a normal or HFD were excised and minced in Krebs-Ringer-bicarbonate-HEPES buffer (KRBH: 120 mM NaCl, 4 mM $KH_2PO_4$, 1 mM $MgSO_4$, 1 mM $CaCl_2$, 10 mM $NaHCO_3$, 30 mM HEPES, 20 μM adenosine (Sigma), 4% BSA). The tissues were then digested with 1 mg ml$^{-1}$ collagenase type II (Sigma) in PBS at 37 °C for 30 min with gentle shaking and filtered through a 100-mm filter. In SVF preparations, the digested cells were separated by centrifugation at 700*g* for 5 min. In MAF preparations, the digested cells were separated by centrifugation at 300*g* for 5 min. The resulting cells were washed twice with KRBH buffer before use in experiments.

**Metabolic measurements.** Serum insulin levels were determined by ELISA (Morinaga Institute of Biological Science Inc.). Serum glucose, NEFA and cholesterol levels were measured with enzymatic kits (WAKO Chemicals). Intraperitoneal glucose tolerance tests were performed on 16 h fasted mice injected intraperitoneally with D-glucose (1.5 mg g$^{-1}$ body weight). Serum glucose levels were measured immediately before administration and 30, 60, 90 and 120 min after the D-glucose injection.

**Lipolysis assay.** *In vivo* lipolysis assays were performed on 4 h fasted mice. Blood was collected from orbital veins, and the serum glycerol and NEFA concentrations were measured. For *ex vivo* assays, adipocytes were isolated from epididymal pads using collagenase, washed twice, re-suspended in Krebs-Ringer buffer at $5 \times 10^5$ cells ml$^{-1}$ and incubated with shaking for the specified times. The glycerol and NEFA concentrations were measured in the supernatants.

**Microarray analysis.** Total RNA was isolated from wild-type and *Trib1*$^{-/-}$ GMP and MDP using TRIzol RNA isolation kit (Invitrogen) and further purified using an RNeasy kit (Qiagen). Biotinylated cDNA was synthesized from 100 ng total RNA with the Ovation biotin RNA amplification and labelling systems (Nugen) according to the manufacturer's protocol. The product was purified using an DyeEx 2.0 spin kit (QIAGEN), fragmented, and hybridized to Affymetrix mouse

expression array A430 2.0 microarray chips, according to the manufacturer's protocol (Affymetrix). Staining, washing and scanning of Affymetrix mouse Genome 430 2.0 microarray chips was done following the manufacturer's instructions. Robust multichip average (RMA) expression values were calculated using R and the Bioconductor affy package. For each probe the changes in expression between wild-type and *Trib1*$^{-/-}$ samples were defined as the difference between $\log_2$ values for wild-type and *Trib1*$^{-/-}$ cells. Genes were assigned the values of their corresponding probe(s). In cases where a gene was associated with multiple probes the average value was taken.

**Statistical analysis.** The statistical significance of differences between values was calculated using the two-tailed Student's *t*-test. Values of $^{*}P < 0.05$, $^{**}P < 0.01$ were considered to indicate statistical significance.

Cardiovascular Research (2013) **99**, 364–373
doi:10.1093/cvr/cvt033

# Toll-like receptor 3 and 4 signalling through the TRIF and TRAM adaptors in haematopoietic cells promotes atherosclerosis

**Anna M. Lundberg[1], Daniel F.J. Ketelhuth[1], Maria E. Johansson[2], Norbert Gerdes[3], Sang Liu[1], Masahiro Yamamoto[4], Shizuo Akira[4], and Göran K. Hansson[1]***

[1]Center for Molecular Medicine, Department of Medicine at Karolinska University Hospital Solna, Karolinska Institutet, Stockholm SE-17176, Sweden; [2]Department of Physiology, Institute of Neuroscience and Physiology, Sahlgrenska Academy, University of Gothenburg, Gothenburg, Sweden; [3]Institute for Cardiovascular Prevention (IPEK), Ludwig-Maximilians-University (LMU), Munich, Germany; and [4]Department of Host Defense, Research Institute for Microbial Diseases, IFReC, Osaka University, 3-1, Yamada-oka, Suita, Osaka, Japan

*Received 4 August 2012; revised 4 January 2013; accepted 1 February 2013; online publish-ahead-of-print 14 February 2013*

**Time for primary review: 31 days**

**Aims** Members of the Toll-like receptor (TLR) family initiate innate immune responses and were recently shown to play a role in atherosclerosis. However, the mechanisms that link TLR ligation to vascular inflammation and atherogenesis remain unclear. To identify which signalling pathways downstream of TLRs in immune cells are pro-atherogenic, we analysed the role of the TLR-specific adaptors MyD88 adaptor-like (MAL), TRIF-related adaptor molecule (TRAM), and TIR-domain-containing adaptor-inducing interferon-β (TRIF) in atherosclerosis.

**Methods and results** Using a bone-marrow transplantation strategy into low-density lipoprotein receptor-deficient ($Ldlr^{-/-}$) mice, we could specifically study the absence of the TLR adaptors in immune cells. We showed that haematopoietic deficiency of TRAM and TRIF, but not MAL, reduces atherosclerosis without affecting cholesterol metabolism. This was mediated by decreased aortic inflammation, indicated by lower aortic levels of pro-inflammatory mediators, and reduced influx of macrophages and T cells. Furthermore, by studying $Tlr3^{-/-}$ chimeric $Ldlr^{-/-}$ mice, we found that deleting TLR3 in immune cells significantly reduced both aortic inflammation and atherosclerotic burden.

**Conclusions** By studying hypercholesterolaemic mice with defects in TLR-signalling adaptors, we demonstrated that deleting either TRAM or TRIF in immune cells is sufficient to attenuate vessel inflammation and protect against atherosclerosis. In addition, these adaptors elicit partly different sets of inflammatory mediators and can independently inhibit the disease process. Furthermore, we identify TLR3 as a pro-atherogenic receptor in haematopoietic immune cells. The identification of these pro-atherogenic pathways downstream of TLR3 and TLR4 contributes to a better understanding of TLRs and their signalling pathways in the pathogenesis of atherosclerosis.

**Keywords** Atherosclerosis • TRAM • TRIF • TLR3 • Vascular inflammation

## 1. Introduction

Atherosclerosis is a chronic inflammatory disorder in which metabolic and immune components interact to initiate and propagate arterial lesions.[1] Immune cells derived from haematopoietic cells in the bone marrow have been identified as key players in driving the disease process. Retention and modification of lipoproteins in the vessel wall lead to attraction of monocytes that eventually differentiate into macrophages. Macrophages are the major immune cells in the lesion and they produce pro-inflammatory cytokines, participate in lipid uptake, and express pattern-recognition receptors, including Toll-like receptors (TLRs) that connect the innate and adaptive immune response during atherosclerosis. TLRs are important for the detection of both pathogenic infections and endogenous danger signals and several lines of evidence have identified them as initiators of inflammation in the lipid-laden artery wall.[2] We have detected several TLRs on activated cells in human atherosclerotic plaques[3] and experimental studies have shown pro-atherogenic effects of TLR2 and TLR4 in hyperlipidaemic mice.[4,5] However, the pathways

* Corresponding author. Tel: +46 8 517 00 00; fax +46 8 313 147, E-mail goran.hansson@ki.se

that link TLRs to pro-atherogenic effectors pathways in immune cells remain poorly characterized.

TLR signalling is controlled by four cytoplasmic receptor adaptors (as reviewed in Akira *et al.*[6]); myeloid differentiation factor 88 (MyD88), MyD88 adaptor-like (MAL), TRIF-related adaptor molecule (TRAM), and TIR-domain-containing adaptor-inducing interferon-β (TRIF) (*Figure 1*). MyD88 mediates signalling from the IL-1/IL-18 receptors and all TLRs except TLR3, whereas MAL facilitates the interaction between MyD88 and the TLR2 and TLR4 receptors. Together, MyD88 and MAL initiate a common pathway that activates nuclear factor (NF)κB. In contrast, TRIF mediates signalling from TLR3 and TLR4, while TRAM operates as a bridging adaptor between TRIF and TLR4. The TRIF- and TRAM-dependent pathways result in activation of both the transcription factor interferon regulatory factor (IRF)-3 and the alternate pathway to NFκB.

Since immune cells within the lesion express many TLRs, it is too simplistic to portray one specific TLR as the sole receptor triggering inflammation during atherogenesis. More likely is a combined involvement of several TLRs in disease development. It is therefore important to determine whether a common pathway downstream of these TLRs is essential for driving lesion inflammation. The role of MyD88 has been investigated and hyperlipidaemic mice deficient in this adaptor protein are protected against disease development.[7,8] However, this could be a consequence of the crucial role of MyD88 in transducing signals from the receptors for IL-1 and IL-18, two well-known pro-atherogenic stimuli.

In the present study, we investigated the TLR-specific adaptor proteins MAL, TRAM, and TRIF in atherosclerosis in low-density lipoprotein receptor (LDLR)-deficient mice. By using a bone-marrow transplantation strategy, we could specifically study the absence of the TLR adaptors in immune cells. We demonstrate that MAL, which controls the signals from TLR2 and TLR4, has a redundant role in disease development. In contrast, TRAM and TRIF that regulate the signalling downstream of the TLR4 and TLR3 receptors were both found to be pro-atherogenic and that these two adaptors regulate lesion inflammation and atherogenesis through separate mechanisms. In addition, we identify TLR3 as a pro-atherogenic receptor in haematopoietic immune cells. Overall, our data indicate that signalling through the TRIF and TRAM pathways downstream of TLR3 and TLR4 in bone-marrow cells promote the development of atherosclerosis.

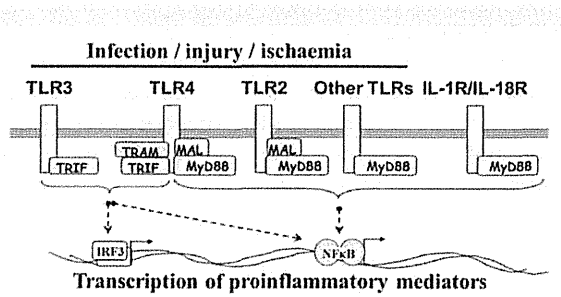


**Figure 1** TLR signalling pathways. TLRs activate common and unique transcription factors, including nuclear factor (NF)κB and interferon regulating factor 3 (IRF-3). Stimulation with TLR ligands, including infectious material and products of tissue stress, results in recruitment of TLR adaptors. TLR3/7/8/9 are expressed in the endosomes (not shown). With the exception of TLR3, all TLRs and IL-1R/IL-18R recruit the adaptor myeloid differentiation factor 88 (MyD88), which signals to activate NFκB. In addition, TLR4 and TLR3 trigger a TIR-domain-containing adaptor-inducing interferon-β (TRIF)-dependent signalling pathway, which induces activation of IRF-3. The adaptors MyD88 adaptor-like (MAL) and TRIF-related adaptor molecule (TRAM) are important for recruiting MyD88 and TRIF to the TLR2 and TLR4 receptors. TLR4, TLR2, IL-1, IL-18, and MyD88 have all been found to mediate pro-atherosclerotic effects.

# 2. Materials and methods

## 2.1 Animals

LDLR-deficient mice were from Jackson Laboratory. MAL, TRAM, and TRIF-deficient mice were generated in the Akira laboratory (Department of Host Defense, Osaka University, Japan). TLR3 mice were kindly provided by Prof. Richard Flavell (Yale University, USA) and Dr Claudia Monaco (Imperial College, UK). The mice were weaned at 4 weeks, and all procedures were approved by the Stockholm North Committee for Experimental Animal Ethics. The investigations conform with the Directive 2010/63/EU of the European Parliament.

## 2.2 Bone-marrow transfer

Bone-marrow transfer (BMT) was performed on female *Ldlr*$^{-/-}$-recipient mice that were irradiated with two doses of 700 rad, 3 h apart. Donor mice were euthanized with $CO_2$ and bone-marrow cells were isolated from the femur and tibia. BMT was performed on the recipients in the absence of anaesthesia through i.v. injection in the tail vein of $5 \times 10^6$ bone-marrow cells per recipient in 50–100 μL. Matched recipients (6–9 weeks old for each study) were randomly assigned to receive bone marrow from *Mal*$^{-/-}$, *Tram*$^{-/-}$, *Trif*$^{-/-}$, *Tlr3*$^{-/-}$ or corresponding C57Bl/6 control female donor mice (6–9 weeks for each study) ($n$ = 7–11 recipients/group) in four separate experiments. Transplanted mice were left to recover for 6 weeks, and following feeding of atherogenic diet (1.25% cholesterol, 0% cholate) (D12108, Research Diets, USA) for 7–8 weeks, mice were terminated within 7 days in matched sets from both experimental and control groups.

## 2.3 Tissue preparation

Mice were euthanized by $CO_2$, blood was saved for serum analysis, and organs were dissected after vascular perfusion. The aorta was cut between the heart and innominate artery and the heart frozen and cryosectioned. The aorta down to the bifurcation was dissected, carefully removing the adventitia, and snap-frozen for RNA isolation.

## 2.4 Lesion analysis and immunohistochemistry

Lesion analysis was performed as described.[9] Briefly, 10 μm sections, collected at 100 μm intervals from 200-μm distance after aortic valve appearance, were fixed (4% formaldehyde) and analysed after oil red-O staining. Images were captured with a Leica DM-LB2 microscope (Leica, Germany) with a ×20/0.9 objective and a Leica DC300 camera. Lesion surface areas and the circumference of the vessel were measured and lesion size was calculated using Leica QWin software. For each mouse, a mean lesion area was calculated from seven sections. Primary rat anti-mouse antibodies to CD68 (BD Bioscience) were applied to acetone-fixed cryosections followed by detection with the ABC alkaline phosphatase kit (Vector Laboratories, USA) and analysed using Leica QWin software.

### 2.5 Cholesterol measurements, lipoprotein lipid profiles and oxLDL measurements

Total serum cholesterol was determined using enzymatic colorimetric kit according to the manufacturers' instructions (Randox Lab. Ltd, UK). Serum cholesterol lipoprotein profiles were determined using UFLC chromatography further described in Supplementary material, Methods. OxLDL serum levels were measured using ELISA (antibodies-online.com) using the manufacturer's' instructions. For oxLDL uptake, cells isolated by peritoneal PBS lavage were stimulated and uptake of FITC-oxLDL was measured as further described in Supplementary material, Methods.

### 2.6 RNA isolation, cDNA synthesis, and real-time PCR analysis

Aortic RNA, prepared using the RNeasy Lipid Mini kit (Qiagen, Germany) and analysed by BioAnalyzer (Agilent Technologies, Germany), were reverse transcribed with Superscript-II (Invitrogen), random hexanucleotide primers (pdN6), and RNasin (Life Technologies, France). cDNA was amplified by real-time PCR using primers and probes (Applied Biosystems, USA) for selected genes and the housekeeping gene hypoxanthine guanidine ribonucleosyltransferase (*Hprt*) in an ABI 7900HT Sequence Detector (Applied Biosystems). Specific mRNA was expressed as arbitrary units calculated as described previously.[10]

### 2.7 *In vivo* stimulation and cytokine measurement

*Trif*$^{-/-}$, *Tram*$^{-/-}$, or control mice were injected with 50 μg LPS (Serotype O111:B4 S-form TL*Rgrade*™, Enzo Life Science) i.p. Blood samples (50 μL) were collected from the tail prior to and 3 and 6 h post LPS injection, and plasma were analysed for cytokines using the Cytokine Bead Array (CBA) detection kit (BD Biosciences, Sweden) or ELISA (R&D Systems, Inc., USA) according to manufacturer's instructions. For CBA, the mean fluorescence intensity (MFI) was measured by a CyanADP flow cytometer (Beckman Coulter, USA) and analysed by FCAP Array™ software (Soft Flow, Inc., USA). The MFI each cytokine was subsequently converted to picograms per millilitre based on MFI values from standards.

### 2.8 Statistical analysis

Results are expressed as mean ± SEM. The Mann–Whitney *U* test was used for pairwise comparisons and two-way ANOVA with Bonferroni post-test was used to compare differences between groups in lesion size plotted as distances from aortic root and lipoprotein lipid profile. Differences between groups were considered significant at $P < 0.05$.

## 3. Results

### 3.1 Haematopoietic deficiency of MAL fails to inhibit atherosclerotic development and lesion inflammation

To study the adaptor MAL in haematopoietic immune cells, which controls signalling from the two pro-atherogenic receptor TLR2 and TLR4, bone-marrow cells from *Mal*$^{-/-}$ or control mice were transplanted into *Ldlr*$^{-/-}$-recipient mice and fed atherogenic diet to induce lesion formation. The resulting fibrofatty lesions in the aortic sinus did not differ in size between *Mal*$^{-/-}$ chimeric mice and controls (*Figure 2A–C*). In addition, no significant changes in either weight, total serum cholesterol (see Supplementary material online, *Table S1*), cholesterol levels in chylomicrons (CR)/VLDL, LDL and HDL (see Supplementary material online, *Figure S1A*), or serum levels of oxLDL (see Supplementary material online, *Figure S2A*) could be observed. Immunohistochemical characterization of the lesions showed similar levels of macrophages independent of MAL expression (*Figure 2D*). Furthermore, aortic expression levels of the key inflammatory cytokines TNF, IL-6, and IFNγ were unchanged between MAL-deficient *Ldlr*$^{-/-}$ chimeric mice and controls (*Figure 2E–G*),.

### 3.2 Disrupted TLR signalling through TRIF and TRAM leads to reduced atherosclerotic burden and decreased macrophage infiltration

Having established that MAL does not play a prominent role in atherogenesis, we investigated the two other TLR-specific adaptors, TRIF and TRAM. We observed that haematopoietic deficiency of either of these two TLR adaptors significantly reduced sinus lesion size compared with control *Ldlr*$^{-/-}$ mice that have intact TLR signalling (*Figure 3A* and *B*). Analysis of lesions in the aortic sinus revealed a decrease of 32.6% in *Tram*$^{-/-}$ chimeric *Ldlr*$^{-/-}$ mice, whereas TRIF deficiency led to an even greater reduction of 40.1% in lesion size compared with controls. Lesion size was uniformly reduced in cross sections throughout the entire aortic sinus in both *Tram*$^{-/-}$ and *Trif*$^{-/-}$ mice (*Figure 3C*). This effect was accompanied by a lower level of macrophage infiltration in both TRIF- and TRAM-deficient chimeric *Ldlr*$^{-/-}$ mice as examined by immunostaining of aortic root lesions (*Figure 3D*). No significant differences in weight, total serum cholesterol (see Supplementary material online, *Table S1*), cholesterol levels in CR/VLDL, LDL, or HDL (see Supplementary material online, *Figure S1B* and *C*), or circulating levels of oxLDL (see Supplementary material online, *Figure S2B* and *C*) were detected.

### 3.3 Differential involvement of TRAM and TRIF in controlling aortic expression of pro-inflammatory mediators and recruitment of macrophages and T cells

To determine whether disrupted TRAM and TRIF signalling in immune cells affected vessel inflammation, we evaluated the aortic expression levels from the adaptor-deficient chimeric *Ldlr*$^{-/-}$ mice and their controls (*Figure 4*). mRNA expression of the Th1-associated cytokine IFNγ and the pro-inflammatory TNF and IL-6 were all significantly decreased in the aorta of mice with *Trif*$^{-/-}$ haematopoietic cells (*Figure 4A*). In contrast, lack of TRAM reduced only expression of IL-6 in the aorta (*Figure 4A*).

We further analysed whether reduction of atherosclerosis was accompanied by changes in cellular composition in the aorta. Aortic infiltration of macrophages as assessed by CD68 expression was significantly lower in *Tram*$^{-/-}$ and *Trif*$^{-/-}$ mice (*Figure 4B*), whereas the levels of the T-cell-specific CD3 transcript were affected only TRIF-deficient chimaeras (*Figure 4B*). These adaptor-specific effects were also reflected in the local production of chemokines that can attract both macrophages and activated T cells. mRNA levels of CCL2, a key chemokine that can regulate migration of monocytes/macrophages, were significantly reduced in both *Tram*$^{-/-}$ and *Trif*$^{-/-}$ mice (*Figure 4C*). In contrast, the expression of the chemokines CCL5 and CXCL10 that can recruit both macrophages and activated T cells during atherosclerosis[11] were abrogated only in TRIF-deficient mice (*Figure 4C*). TRAM is commonly believed to function exclusively in combination with TRIF; however, our data suggest that TRAM and TRIF have independent roles in initiating aortic inflammation.

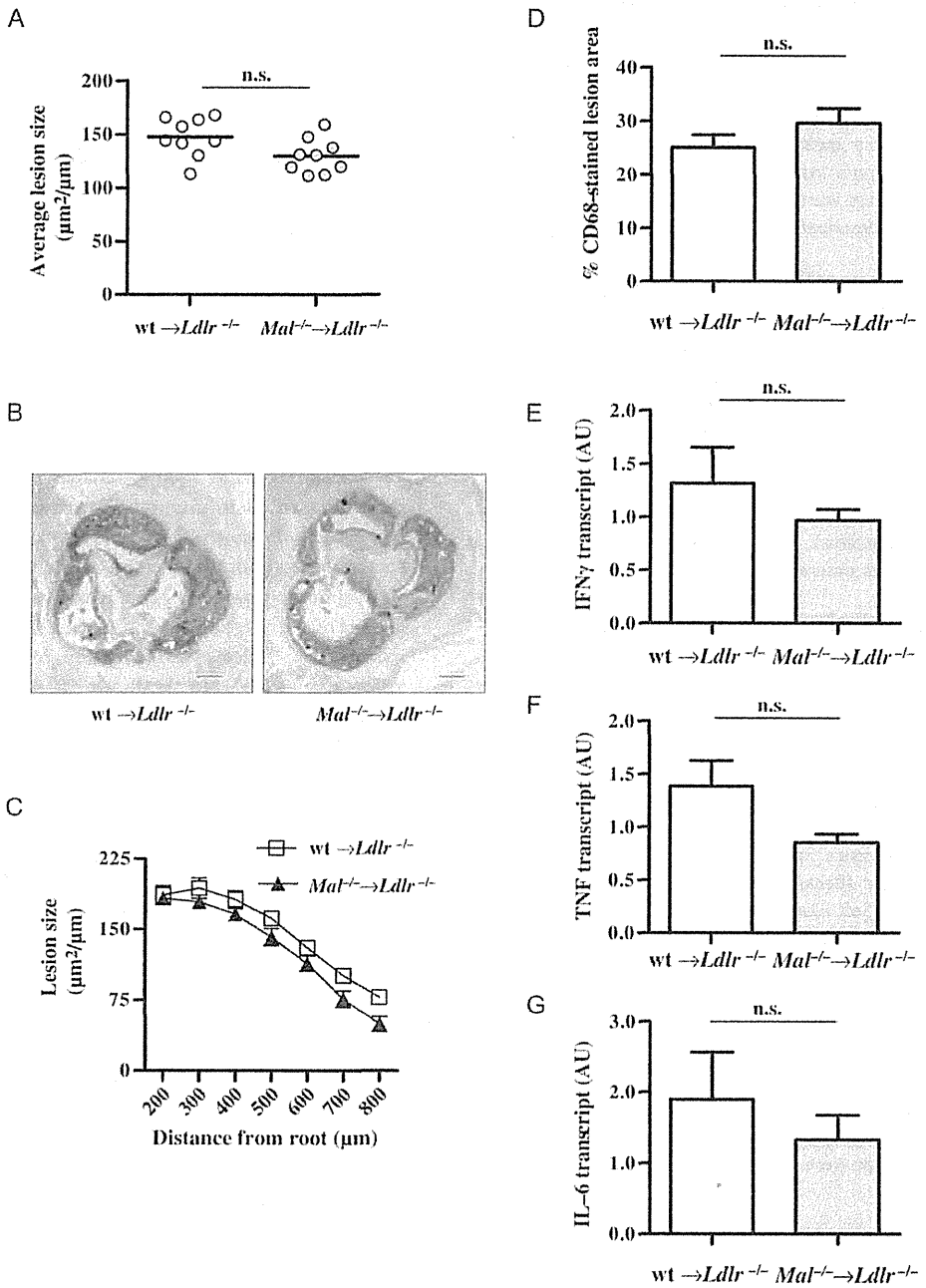


**Figure 2** MAL deficiency does not affect atherosclerosis or aortic inflammation. Aortic root lesions, from $Ldlr^{-/-}$ mice transplanted with bone marrow of control or $Mal^{-/-}$ mice and fed an atherogenic diet, were evaluated by microscopic morphometry of serial sections after staining with Oil Red O. (*A*) Average lesion size at 200–800 μm from the aortic root is shown, calculated as size covered by lesion ($\mu m^2$) related to the aortic perimeter (μm). Individual values are displayed by dots, and the mean for each group indicated by horizontal lines. (*B*) Representative micrographs showing cross sections of Oil Red O-stained lesion 400 μm from the start of the aortic root (black bar 25 μm). (*C*) Lesion size measured on serial sections throughout the proximal aorta. (*D*) Graph shows an average lesion area as proportion of total lesion area stained by CD68 antibody in aortic root sections from control or $Mal^{-/-}$ mice. Relative mRNA levels of (*E*) IFN-γ, (F) TNF, and (*G*) IL-6 mRNA normalized to *Hprt* in aorta from the two groups analysed with reverse-transcription real-time PCR. Data expressed as arbitrary units (AU). n.s., non-significant.

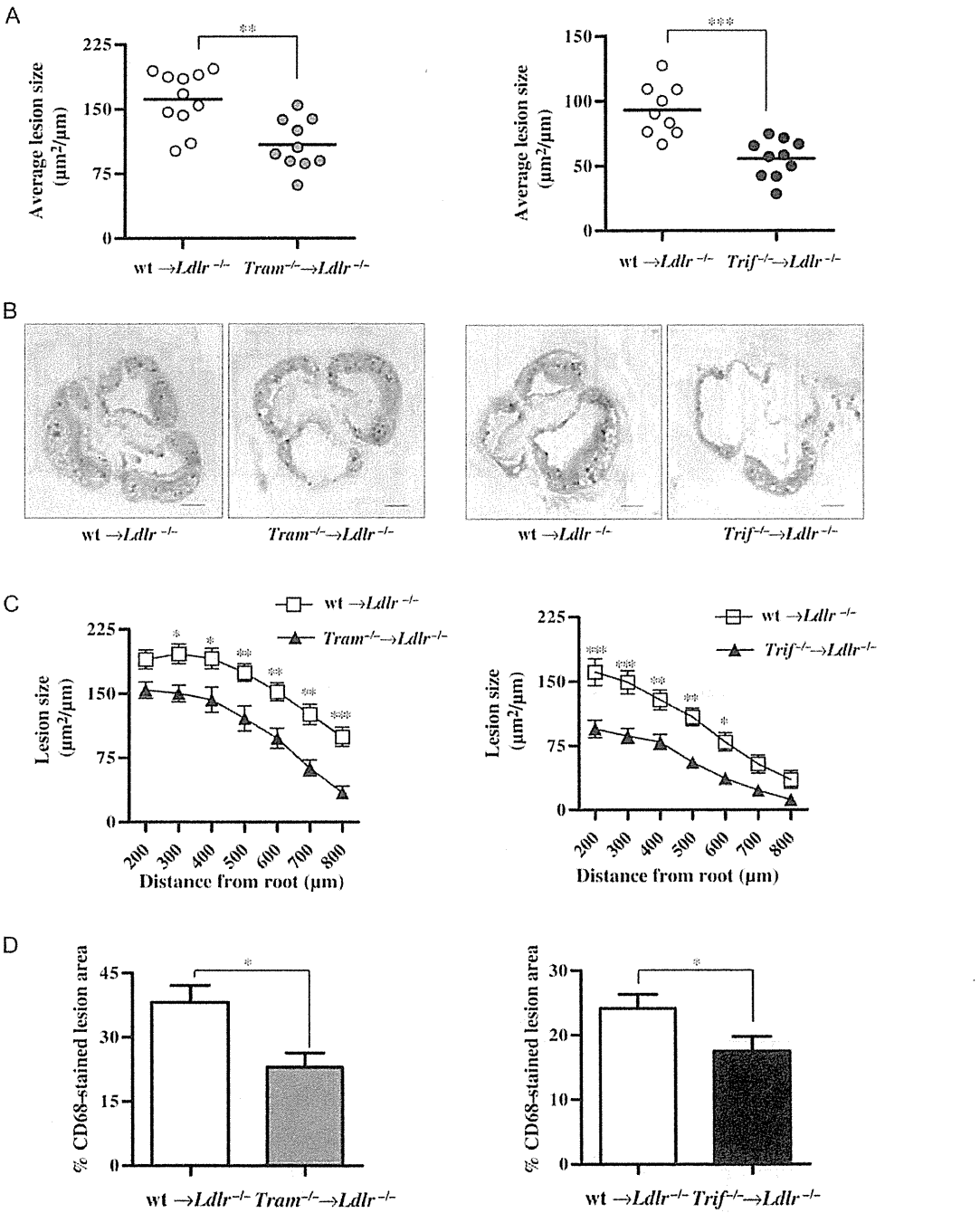


**Figure 3** Atherosclerotic burden is reduced in TRIF and TRAM-defective mice. Quantitative Oil Red O lesion analysis in aortic root cross sections of control, *Tram*$^{-/-}$, or *Trif*$^{-/-}$ chimeric *Ldlr*$^{-/-}$ mice fed an atherogenic diet using microscopic morphometry of serial sections. (*A*) Average lesion size at 200–800 μm from the aortic root is shown, calculated as size covered by lesion (μm$^2$) related to the aortic perimeter (μm). Individual values are displayed by dots, and the mean for each group indicated by horizontal lines. (*B*) Representative micrographs showing cross sections of Oil Red O-stained lesion at 400 μm (black bar 25 μm). (*C*) Lesion size measured in throughout the proximal aorta. (*D*) Graph shows an average lesion area as the proportion of total lesion area stained by CD68 antibody in aortic root sections. n.s., non-significant. *$P$<0.05, **$P$ < 0.01, and ***$P$ < 0.001.

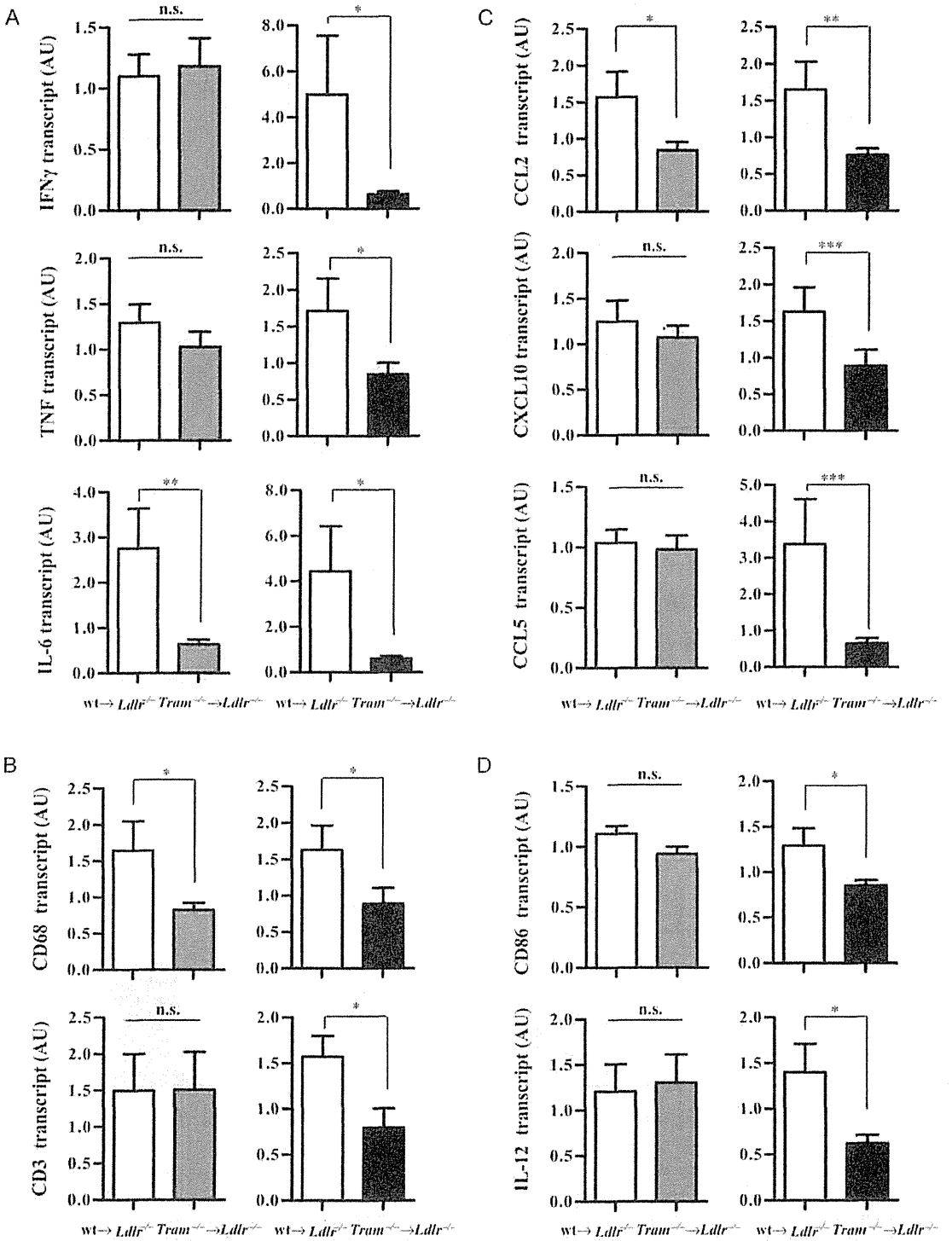


**Figure 4** TRIF and TRAM deficiencies differentially regulate aortic pro-inflammatory mediators and influx of macrophage and T cells. Aortic mRNA transcripts from control, $Tram^{-/-}$ or $Trif^{-/-}$ chimeric $Ldlr^{-/-}$ mice were analysed with reverse-transcription real-time PCR and normalized to *Hprt*. Data are expressed as arbitrary units (AU). n.s., non-significant. $^{*}P<0.05$, $^{**}P<0.01$, $^{***}P<0.001$.

We assessed whether TRIF or TRAM deficiency could affect mediators of antigen presentation in the atherosclerotic aorta. mRNA expression of the important co-stimulatory B7.2 (CD86) molecule that ligates CD28 on the T cells and the Th1 polarizing cytokine IL-12 were both reduced in the aorta of mice with TRIF deficiency, whereas impaired TRAM-signalling had no effect (*Figure 4D*).

Next, the effect of TRIF and TRAM deficiency on the oxLDL uptake by macrophages was studied. No significant differences could be observed in the uptake of FITC-labelled oxLDL by peritoneal macrophages from *Tram*$^{-/-}$ and *Trif*$^{-/-}$ mice when compared with controls (see Supplementary material online, *Figure S3A*). Moreover, aortic expression of the cholesterol efflux transporter, ATP-binding cassette transporter A (ABCA)-1, were unchanged between *Tram*$^{-/-}$ and *Trif*$^{-/-}$ chimeric *Ldlr*$^{-/-}$ mice and their controls (see Supplementary material online, *Figure S3B*).

### 3.4 TRAM and TRIF regulate inflammatory gene expression in a stimulus-dependent manner

Having established that the TLR-pathways mediated by TRAM and TRIF are both pro-atherogenic, we next aimed to address the basis for their different activation patterns. The contributing roles between TRIF and TRAM in TLR4 signalling have not been directly compared, thus the dissimilarities could be the results of the adaptors activating different pathways downstream of TLR4. We tested this by injecting LPS in control, *Trif*$^{-/-}$, or *Tram*$^{-/-}$ mice to determine the relative involvement of the two adaptors in TLR4-induced cytokine production. As expected, in the control mice, circulating levels of TNF and IL-12 peaked at 3 h post LPS injection and were declining at 6 h (*Figure 5A* and *B*). While these two cytokines could also be detected in plasma of both TRIF and TRAM-deficient mice, the levels were markedly reduced at 3 h and almost absent at 6 h post LPS stimulation. In contrast, secretion of IFNγ was similar in all mice at 3 h whereas both TRIF and TRAM deficiency caused a reduction at 6 h (*Figure 5C*), indicating that only the late phase of IFNγ secretion depends on the TRIF and TRAM pathways. Both adaptors were able to block the LPS-induced secretion of the chemokines, CCL2, CXCL10, and CCL5 (*Figure 5D–F*), to a similar extent. Taken together, both TRIF and TRAM were equally able to inhibit LPS-induced responses *in vivo* in a non-compensatory manner, in contrast to the results obtained in the atherosclerotic model.

### 3.5 TLR3 deficiency in haematopoietic cells protects against atherosclerosis in Ldlr$^{-/-}$ mice

While both adaptors are utilized by TLR4, TRIF is the only adaptor employed by TLR3. Therefore, TRIF deficiency might block both TLR4 and TLR3, while the absence of TRAM would only block TLR4, a possible explanation for the observed differences. Using BMT from *Tlr3*$^{-/-}$ donors into *Ldlr*$^{-/-}$ recipients, we observed that haematopoietic deficiency of TLR3 significantly reduced the lesion size in the aortic sinus by 43.9% (*Figure 6A* and *B*). The lesions were uniformly reduced in cross sections of the aortic sinus in the TLR3-deficient *Ldlr*$^{-/-}$ mice (*Figure 6C*). In addition, aortic transcript levels of the macrophage and T-cell markers CD68 and CD3 were decreased (*Figure 6D* and *E*), as well as mRNA for the pro-inflammatory cytokines, TNF and IFNγ (*Figure 6F* and *G*). There was no significant change in either weight, total serum cholesterol (see Supplementary material online, *Table S2*), cholesterol levels in CR/VLDL, LDL, and HDL (see Supplementary material online, *Figure S1C*), or serum levels of oxLDL (see Supplementary material online, *Figure S2C*) observed when compared with controls.

## 4. Discussion

Atherosclerotic lesions are characterized by cell death and accumulation of lipids, likely generating a co-ordinated response from several TLRs. This stimulation initiates both common and unique signalling pathways, which decide the pattern of gene expression elicited, and the recruitment and activation of immune cells. It is therefore important to identify the TLR adaptor proteins causing increased inflammation in the plaque.

Our data show that signalling through TRAM and TRIF, but not MAL, adaptors in haematopoietic immune cells are pro-atherogenic in hyperlipidaemic *Ldlr*$^{-/-}$ mice. This was not due to altered serum cholesterol, or changes in levels of CR/VLDL, LDL, HDL, but associated with reduced vascular inflammation. Bone-marrow chimaeras of *Trif*$^{-/-}$ and *Tram*$^{-/-}$ displayed reduced levels of macrophages and CCL2 in the lesions. CCL2 and CCL5, strikingly impaired only in *Trif*$^{-/-}$ chimeric mice, are both involved in recruitment of macrophages. This suggests that TRIF- and TRAM-dependent signalling in haematopoietic immune cells increases atherosclerosis by promoting recruitment of macrophages to the plaque.

*Trif*$^{-/-}$ and *Tram*$^{-/-}$ chimeric mice also displayed decreased aortic expression of pro-inflammatory cytokines. Interestingly, TRAM appeared to regulate a distinct signalling pathway. While TRIF deficiency reduced both TNF and IL-6, mice lacking TRAM only had lower IL-6 levels. Furthermore, *Trif*$^{-/-}$ chimeric mice had reduced mRNA levels for the T-cell-specific CD3 marker, probably a consequence of the diminished levels CCL5 and CXCL10 in the TRIF-deficient mice. These chemokines are involved in T-cell recruitment and mice deficient in CXCL10 or the CCL5 receptor CCR5 have impaired T-cell accumulation and reduced atherosclerosis.[12,13]

The Th1 subtype is the dominating T-cell population in the atherosclerotic plaque and can aggravate atherosclerosis in part through secretion of IFNγ. This Th1 cytokine pattern is predominantly induced by IL-12, which also contributes to the development of atherosclerosis. In our study, both IFNγ and IL-12 production was reduced in the *Trif*$^{-/-}$ mice paralleled by reduced aortic expression of CD86, a critical co-stimulatory molecule in the initiation of adaptive immunity. Mice lacking TRIF in haematopoietic immune cells displayed a more pronounced reduction of atherosclerosis which might be explained by the impaired recruitment and Th1 effector function of T cells in the lesion. In support of this, the TRIF pathway was recently shown to be critical for effector T-cell accumulation into non-lymphoid tissues following an induced immune response.[14]

In contrast to TRIF and TRAM, chimeric MAL-deficient mice showed no significant inhibition of any parameter measured in this study. Thus, our findings argue against a pro-atherogenic role for MAL signalling in haematopoietic immune cells, although a compensatory effect by MyD88, or the other adaptors, cannot be excluded in the absence of MAL. However, the discrepancy between MAL in comparison with TRIF and TRAM suggests that activation of the transcription factor IRF3, which is induced by TRIF and TRAM, is needed to mediate a more important pro-atherogenic signal. MAL which does not lead to IRF-3 activation would therefore not provide this signal.

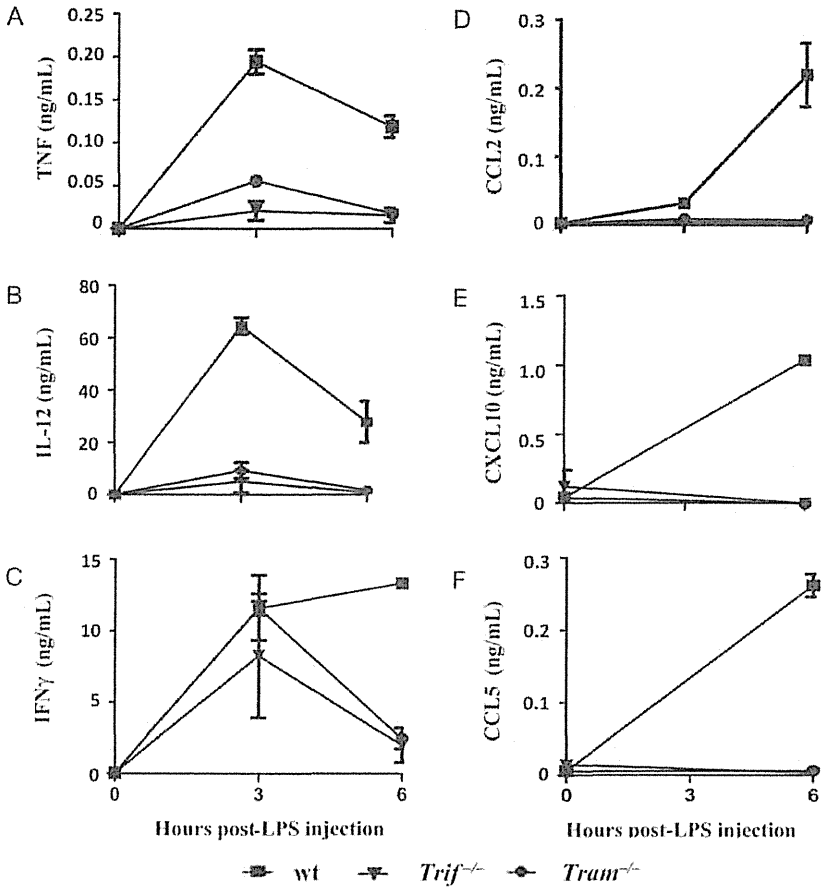


**Figure 5** TRIF and TRAM both control TLR4-dependent cytokine production in a non-compensatory manner. *Tram*$^{-/-}$ (squares), *Trif*$^{-/-}$ (inverted triangles), or control mice (circles) were injected with 50 μg LPS i.p. Blood samples were collected prior to, 3 and 6 h post LPS injection and plasma were analysed for (*A*) TNF, (*B*) IL-12, (*C*) IFNγ, (*D*) CCL2, (*E*) CXCL10, (*F*) CCL5 using CBA and ELISA. Values are represented as mean ± SEM from three to four mice per point.

This would be in line with the recent finding that type I IFNs that are induced by IRF3 promote atherosclerosis by stimulating macrophage recruitment to lesions.[15]

Our finding that TRIF signalling in haematopoietic immune cells drives this disease is supported by a recent report published during the preparation of this manuscript, showing that a global deficiency of the *Lps2* mutation in TRIF was atheroprotective in *Ldlr*$^{-/-}$ mice. We take this further by showing that a specific deletion of TRIF in bone-marrow immune cells is sufficient to inhibit atherogenesis. In addition, we demonstrate that haematopoetically expressed TRAM has an independent role in the disease process and blocking this protein is enough to inhibit the disease process.

The mechanism behind the differences between TRIF- and TRAM-deficient mice is unclear. TRIF and TRAM are proposed to cooperate in the induction of downstream signalling from TLR4.[16] However, since TRAM has not been extensively studied, it cannot be excluded that it has a function separate from TRIF downstream of TLR4, therefore we cannot rule out that an athero-specific TLR4 ligand could selectively signal through only one adaptor. Recent evidence indicates that certain TLR4 ligands can specifically initiate only TRIF-selective signalling,[17] and in the context of atherosclerosis stimulation by the two TLR4 ligands, LPS and minimally modified LDL result in differences in cell activation.[18] It is unclear which TLR ligands are driving the disease in our study, however, using the prototypic TLR4 ligand LPS, we show that TRIF and TRAM are equally important for the secretion of pro-inflammatory cytokines and chemokines *in vivo*. This indicates that in the case of LPS they regulate the same pathway downstream of TLR4 and do not compensate for each other.

Alternatively, the differences between the two adaptors might be caused by activation of different TLR receptors in the lesion, where TRIF deletion would affect both TLR4 and TLR3 receptors, while absence of TRAM would only inhibit TLR4. TRIF is the sole adaptor utilized by the TLR3 receptor and, to further investigate this pathway, we analysed the role of TLR3 in experimental atherosclerosis. Similar to mice lacking TRIF, TLR3-deficient chimeric *Ldlr*$^{-/-}$ mice exhibited reduced atherosclerotic burden. Furthermore, the aortic levels of the macrophage and T-cell markers were inhibited along with the cytokines TNF and IFNγ, indicating a lower level of aortic inflammation. These results match the findings observed in the TRIF-deficient mice and suggest that TRIF mediates its pro-atherogenic role downstream of TLR3 in haematopoietic immune cells.

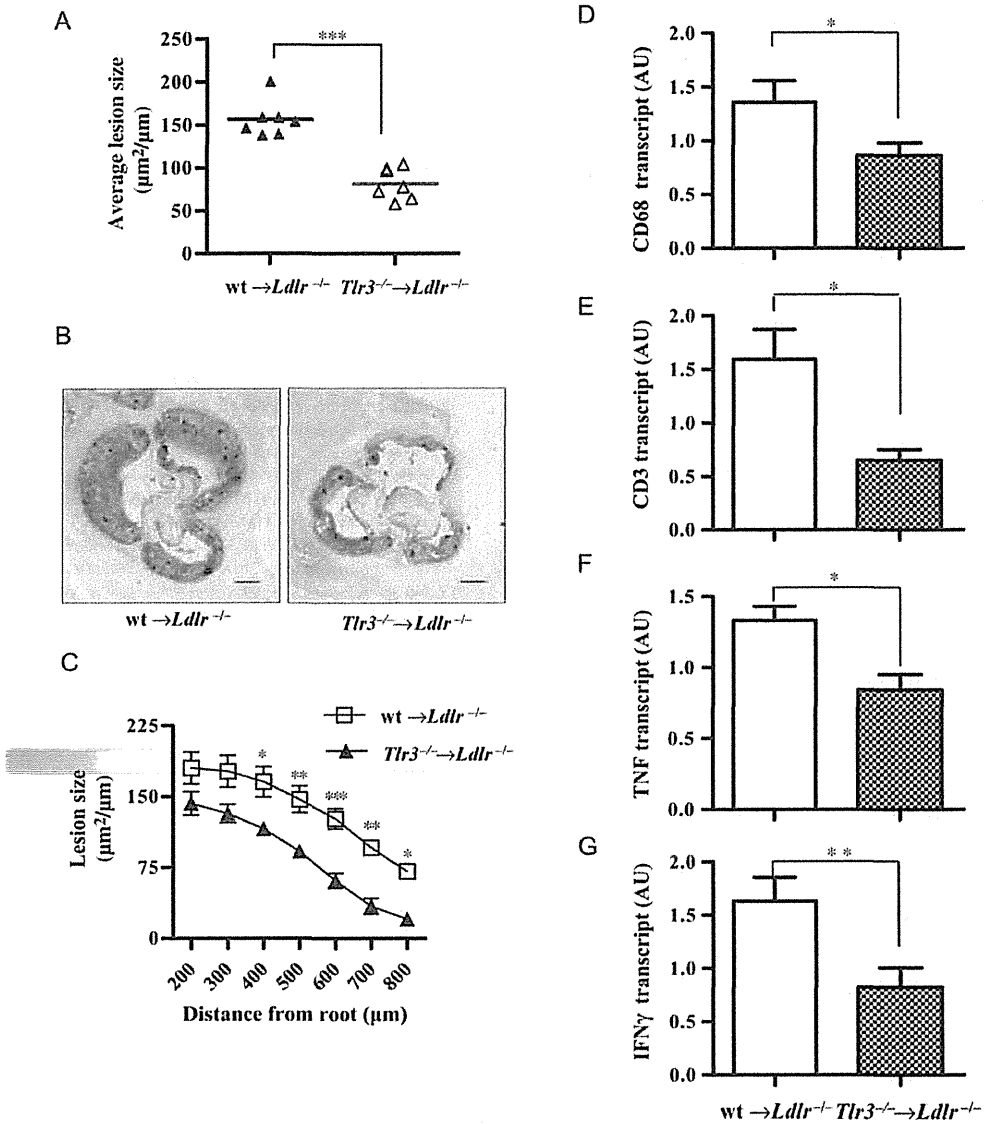


**Figure 6** Haematopoietically expressed TLR3 is pro-atherogenic in LDLR-deficient mice. Quantitative lesion analysis in aortic root cross sections of control or *Tlr3*$^{-/-}$ chimeric *Ldlr*$^{-/-}$ mice fed an atherogenic diet evaluated by microscopic morphometry of serial sections. (*A*) The average lesion size at 200–800 μm from the aortic root is shown, calculated as size covered by lesion (μm$^2$) related to the aortic perimeter (μm). Individual values are displayed by dots, and the mean for each group indicated by horizontal lines. (*B*) Representative micrographs showing cross sections of Oil Red O-stained lesions at 400 μm (black bar 25 μm). (*C*) Lesion size throughout the proximal aorta. Relative mRNA levels of (*D*) CD68, (*E*) CD3, (*F*) TNF, and (*G*) IFNγ in aorta were analysed with real-time PCR and normalized to *Hprt*. Data are expressed as arbitrary units (AU). **P*<0.05, ***P* < 0.01, and ****P* < 0.001.

The TLR3-activating ligands in the atherosclerotic lesion remain to be identified. TLR3 is triggered by stimulation with dsRNA and reported to be an endogenous sensor of tissue necrosis,[19] probably through the detection of host-derived RNA from necrotic cells.[20] The presence of cell death material in the necrotic core makes this a plausible way for TLR3 activation within the lesion. However, even though there were signs of activity within the lesion in our chimeric *Tlr3*$^{-/-}$ mice, one cannot exclude a systemic effect.

Our study identifies TLR3 signalling in cells of the haematopoietic compartment as atherogenic. Both macrophages and dendritic cells express high levels of TLR3 and could be activated through stimulation via the receptor. Furthermore, TLR3 is expressed on certain T-cell subsets but cannot alone induce T-cell activation. Instead, TLR3 ligation can mediate co-stimulation with TCR in human γδ T cells[21] and to a small extent in αβ T cells.[22] Given that γδ T cells play only a minor role in the plaque,[23] TLR3-induced γδ T-cell stimulation probably does not impact on the results in this study. However, based on our experimental set up, we cannot rule out a co-stimulatory effect on T cells.

Conflicting data regarding the role of TLR3 in atherosclerosis were recently reported.[24–26] Whole-body knockout of TLR3 in *Apoe*$^{-/-}$ mice exhibit increased atherosclerosis at early stages whereas this

effect was lost at more advanced stages of the disease.[24] In addition, similar results were reported during the preparation of this manuscript in compound mutant mice lacking *Ldlr* and *Tlr3*.[26] In contrast to these findings and in line with our results, Zimmer *et al.* show that atherosclerotic plaque development is increased by TLR3 stimulation in *Apoe*$^{-/-}$ mice, suggesting a pro-atherogenic role for TLR3.[25] It is likely that TLR3 exerts different responses depending whether the cell is of haematopoietic origin or not, similar to TLR2.[4] This would also be in agreement with our previous report showing that human haematopoietic cells react differently to TLR3 ligands than non-haematopoietic cells.[27] In addition, our finding of a pro-atherogenic role for bone-marrow-derived TLR3 is in line with the effects of its adaptor TRIF in haematopoietic cells, and also with several cell culture studies showing pro-atherogenic effects of TLR3 ligation on such cells, including impaired cholesterol efflux, increased inflammation, and enhanced protease secretion.[28–30]

In summary, our results demonstrate that haematopoietic abrogation of the TLR-signalling pathways involving TLR3, TRIF, and TRAM reduces vascular inflammation and inhibits the development of atherosclerosis. These TLR-signalling pathways elicit partly different sets of pro-atherogenic mediators, and can independently inhibit the disease process. The identification of these pro-atherogenic pathways contributes to our understanding of the innate mechanisms at play during atherogenesis and points to TLR signal transduction in haematopoietic immune cells as a possible therapeutic target in atherosclerotic cardiovascular disease.

## Supplementary material

Supplementary material is available at *Cardiovascular Research* online.


## Acknowledgements

We thank Ingrid Törnberg, Anneli Olsson, Inger Bodin, and André Strodthoff for technical assistance and Prof. R. Flavell (Yale University, USA) and Dr Claudia Monaco (Imperial College, UK) for kindly providing the TLR3-deficient mice.

**Conflict of interest:** none declared.

## Funding

This work was supported by grants from the Swedish Research Council (grants 6816 and 8703); the Swedish Heart-Lung Foundation; the European Commission (AtheroRemo collaborative project); the Foundation for Strategic Research; Vinnova Foundation, Stockholm County Council; Konung Gustaf V:s 80-years fond; Loo and Osterman's foundation; O. E. and Edla Johansson's Foundation; Magnus Bergvall's Foundation; Prof. Nanna Svartz Foundation; Gun and Bertil Stohne's Foundation, and KI Foundations for Geriatric Research.


## References


1. Hansson GK. Inflammation, atherosclerosis, and coronary artery disease. *N Engl J Med* 2005;**352**:1685–1695.
2. Lundberg AM, Hansson GK. Innate immune signals in atherosclerosis. *Clin Immunol* 2010;**134**:5–24.
3. Edfeldt K, Swedenborg J, Hansson GK, Yan ZQ. Expression of toll-like receptors in human atherosclerotic lesions: a possible pathway for plaque activation. *Circulation* 2002;**105**:1158–1161.
4. Mullick AE, Tobias PS, Curtiss LK. Modulation of atherosclerosis in mice by Toll-like receptor 2. *J Clin Invest* 2005;**115**:3149–3156.
5. Michelsen KS, Wong MH, Shah PK, Zhang W, Yano J, Doherty TM *et al.* Lack of Toll-like receptor 4 or myeloid differentiation factor 88 reduces atherosclerosis and alters plaque phenotype in mice deficient in apolipoprotein E. *Proc Natl Acad Sci USA* 2004;**101**:10679–10684.
6. Akira S, Uematsu S, Takeuchi O. Pathogen recognition and innate immunity. *Cell* 2006;**124**:783–801.
7. Michelsen KS, Aicher A, Mohaupt M, Hartung T, Dimmeler S, Kirschning CJ *et al.* The role of toll-like receptors (TLRs) in bacteria-induced maturation of murine dendritic cells (DCS). Peptidoglycan and lipoteichoic acid are inducers of DC maturation and require TLR2. *J Biol Chem* 2001;**276**:25680–25686.
8. Bjorkbacka H, Kunjathoor VV, Moore KJ, Koehn S, Ordija CM, Lee MA *et al.* Reduced atherosclerosis in MyD88-null mice links elevated serum cholesterol levels to activation of innate immunity signaling pathways. *Nat Med* 2004;**10**:416–421.
9. Nicoletti A, Kaveri S, Caligiuri G, Bariety J, Hansson GK. Immunoglobulin treatment reduces atherosclerosis in apo E knockout mice. *J Clin Invest* 1998;**102**:910–918.
10. Zhang L, Ovchinnikova O, Jonsson A, Lundberg AM, Berg M, Hansson GK *et al.* The tryptophan metabolite 3-hydroxyanthranilic acid lowers plasma lipids and decreases atherosclerosis in hypercholesterolaemic mice. *Eur Heart J* 2012;**33**:2025–2034.
11. Zernecke A, Shagdarsuren E, Weber C. Chemokines in atherosclerosis: an update. *Arterioscler Thromb Vasc Biol* 2008;**28**:1897–1908.
12. Braunersreuther V, Steffens S, Arnaud C, Pelli G, Burger F, Proudfoot A *et al.* A novel RANTES antagonist prevents progression of established atherosclerotic lesions in mice. *Arterioscler Thromb Vasc Biol* 2008;**28**:1090–1096.
13. Heller EA, Liu E, Tager AM, Yuan Q, Lin AY, Ahluwalia N *et al.* Chemokine CXCL10 promotes atherogenesis by modulating the local balance of effector and regulatory T cells. *Circulation* 2006;**113**:2301–2312.
14. McAleer JP, Rossi RJ, Vella AT. Lipopolysaccharide potentiates effector T cell accumulation into nonlymphoid tissues through TRIF. *J Immunol* 2009;**182**:5322–5330.
15. Goossens P, Gijbels MJ, Zernecke A, Eijgelaar W, Vergouwe MN, van der Made I *et al.* Myeloid type I interferon signaling promotes atherosclerosis by stimulating macrophage recruitment to lesions. *Cell Metab* 2010;**12**:142–153.
16. Oshiumi H, Sasai M, Shida K, Fujita T, Matsumoto M, Seya T. TIR-containing adapter molecule (TICAM)-2, a bridging adapter recruiting to toll-like receptor 4 TICAM-1 that induces interferon-beta. *J Biol Chem* 2003;**278**:49751–49762.
17. Bowen WS, Minns LA, Johnson DA, Mitchell TC, Hutton MM, Evans JT. Selective TRIF-dependent signaling by a synthetic Toll-like receptor 4 agonist. *Science Signal* 2012;**5**:ra13.
18. Miller YI, Viriyakosol S, Worrall DS, Boullier A, Butler S, Witztum JL. Toll-like receptor 4-dependent and -independent cytokine secretion induced by minimally oxidized low-density lipoprotein in macrophages. *Arterioscler Thromb Vasc Biol* 2005;**25**:1213–1219.
19. Cavassani KA, Ishii M, Wen H, Schaller MA, Lincoln PM, Lukacs NW *et al.* TLR3 is an endogenous sensor of tissue necrosis during acute inflammatory events. *J Exp Med* 2008;**205**:2609–2621.
20. Kariko K, Ni H, Capodici J, Lamphier M, Weissman D. mRNA is an endogenous ligand for Toll-like receptor 3. *J Biol Chem* 2004;**279**:12542–12550.
21. Beetz S, Wesch D, Marischen L, Welte S, Oberg HH, Kabelitz D. Innate immune functions of human gammadelta T cells. *Immunobiology* 2008;**213**:173–182.
22. Meyer T, Oberg HH, Peters C, Martens I, Adam-Klages S, Kabelitz D *et al.* poly(I:C) costimulation induces a stronger antiviral chemokine and granzyme B release in human CD4 T cells than CD28 costimulation. *J Leukoc Biol* 2012;**92**:765–774.
23. Elhage R, Gourdy P, Brouchet L, Jawien J, Fouque MJ, Fievet C *et al.* Deleting TCR alpha beta+ or CD4+ T lymphocytes leads to opposite effects on site-specific atherosclerosis in female apolipoprotein E-deficient mice. *Am J Pathol* 2004;**165**:2013–2018.
24. Cole JE, Navin TJ, Cross AJ, Goddard ME, Alexopoulou L, Mitra AT *et al.* From the cover: unexpected protective role for Toll-like receptor 3 in the arterial wall. *Proc Natl Acad Sci USA* 2011;**108**:2372–2377.
25. Zimmer S, Steinmetz M, Asdonk T, Motz I, Coch C, Hartmann E *et al.* Activation of endothelial toll-like receptor 3 impairs endothelial function. *Circ Res* 2011;**108**:1358–1366.
26. Richards MR, Black AS, Bonnet DJ, Barish GD, Woo CW, Tabas I *et al.* The LPS2 mutation in TRIF is atheroprotective in hyperlipidemic low density lipoprotein receptor knockout mice. *Innate Immun* 2013;**19**:20–9.
27. Lundberg AM, Drexler SK, Monaco C, Williams LM, Sacre SM, Feldmann M *et al.* Key differences in TLR3/poly I:C signaling and cytokine induction by human primary cells: a phenomenon absent from murine cell systems. *Blood* 2007;**110**:3245–3252.
28. Ahmad U, Ali R, Lebastchi AH, Qin L, Lo SF, Yakimov AO *et al.* IFN-gamma primes intact human coronary arteries and cultured coronary smooth muscle cells to double-stranded RNA- and self-RNA-induced inflammatory responses by upregulating TLR3 and melanoma differentiation-associated gene 5. *J Immunol* 2010;**185**:1283–1294.
29. Alexopoulou L, Holt AC, Medzhitov R, Flavell RA. Recognition of double-stranded RNA and activation of NF-kappaB by Toll-like receptor 3. *Nature* 2001;**413**:732–738.
30. Castrillo A, Joseph SB, Vaidya SA, Haberland M, Fogelman AM, Cheng G *et al.* Crosstalk between LXR and toll-like receptor signaling mediates bacterial and viral antagonism of cholesterol metabolism. *Mol Cell* 2003;**12**:805–816.

PLOS | ONE

# CREBH Determines the Severity of Sulpyrine-Induced Fatal Shock

**Naganori Kamiyama[1,2,3,4☯], Masahiro Yamamoto[1,2,3,4,5*☯], Hiroyuki Saiga[1,2], Ji Su Ma[1,2,3,4], Jun Ohshima[1,2,3,4], Sakaaki Machimura[1,2,3,4], Miwa Sasai[3,4], Taishi Kimura[1,2], Yoshiyasu Ueda[1,2], Hisako Kayama[1,2,5], Kiyoshi Takeda[1,2,5*]**

**1** Department of Microbiology and Immunology, Graduate School of Medicine, Osaka University, Suita, Osaka, Japan, **2** Laboratory of Mucosal Immunology, WPI Immunology Frontier Research Center, Osaka University, Suita, Osaka, Japan, **3** Laboratory of Immunoparasitology, WPI Immunology Frontier Research Center, Osaka University, Suita, Osaka, Japan, **4** Department of Immunoparasitology, Research Institute for Microbial Diseases, Osaka University, Suita, Osaka, Japan, **5** Core Research for Evolutional Science and Technology, Japan Science and Technology Agency, Kawaguchi, Saitama, Japan

## Abstract

Although the pyrazolone derivative sulpyrine is widely used as an antipyretic analgesic drug, side effects, including fatal shock, have been reported. However, the molecular mechanism underlying such a severe side effect is largely unclear. Here, we report that the transcription factor CREBH that is highly expressed in the liver plays an important role in fatal shock induced by sulpyrine in mice. CREBH-deficient mice were resistant to experimental fatal sulpyrine shock. We found that sulpyrine-induced expression of cytochrome P450 2B (CYP2B) family genes, which are involved in sulpyrine metabolism, in the liver was severely impaired in CREBH-deficient mice. Moreover, introduction of CYP2B in CREBH-deficient liver restored susceptibility to sulpyrine. Furthermore, ectopic expression of CREBH up-regulated CYP2B10 promoter activity, and *in vivo* knockdown of CREBH in wild-type mice conferred a significant resistance to fatal sulpyrine shock. These data demonstrate that CREBH is a positive regulator of CYP2B in response to sulpyrine administration, which possibly results in fatal shock.

**Citation:** Kamiyama N, Yamamoto M, Saiga H, Ma JS, Ohshima J, et al. (2013) CREBH Determines the Severity of Sulpyrine-Induced Fatal Shock. PLoS ONE 8(2): e55800. doi:10.1371/journal.pone.0055800

**Editor:** Wendong Huang, Beckman Research Institute of City of Hope, United States of America

**Received** September 13, 2012; **Accepted** January 2, 2013; **Published** February 7, 2013



**Funding:** This work was supported by grants from the Ministry of Education, Culture, Sports, Science and Technology, the Strategic International Cooperative Program (Research Exchange Type), the Japan Science and Technology Agency (JST), and; Kato Memorial Bioscience Foundation; Mochida Memorial Foundation for Medical and Pharmaceutical Research; The Waksman Foundation of Japan INC, Senri Life Science Foundation; The Tokyo Biochemical Research Foundation; The Research Foundation for Microbial Diseases of Osaka University; THE NAKAJIMA FOUNDATION; THE ASAHI GLASS FOUNDATION; The Osaka Foundation for Promotion of Clinical Immunology; The Sumitomo Foundation; The Sagawa Foundation of Promotion of Cancer Research; Suzuken Memorial Foundation; Osaka Cancer Research Foundation. The funders had no role in study design, data collection and analysis, decision to publish, or preparation of the manuscript.

**Competing Interests:** The authors have declared that no competing interests exist.

* E-mail: myamamoto@biken.osaka-u.ac.jp (MY); ktakeda@ongene.med.osaka-u.ac.jp (KT)

☯ These authors contributed equally to this work.

## Introduction

Endoplasmic reticulum (ER) is a cytoplasmic organelle, which plays an important role in folding and assembly of newly synthesized proteins [1]. Accumulation of misfolded or unfolded proteins in ER induces ER stress and results in refolding or degradation of the proteins, which is termed unfolded protein response (UPR). The UPR has been shown to involve three major pathways dependent on ATF6α, IRE1α/β-XBP1, or PERK [2]. IRE1α and IRE1β are ER-localizing endonucleases, which catalyze the splicing of the XBP1 mRNA resulting in the frame shift and production of the active form of XBP1 inducing various proteins involved in UPR [3]. PERK is a kinase that phosphorylates eIF2a, leading to translational inhibition to reduce global protein loading [4]. The ATF6α-dependent pathway is regulated by the transcription factor ATF6α, which is localized in ER in unstimulated conditions [5]. In response to ER stress, ATF6α moves from ER to the Golgi apparatus, where it is cleaved by site-specific proteases, S1P and S2P, liberating the N-terminal basic leucine zipper (b-ZIP) and the transcription activation domains to the nucleus. The translocation of the N-terminus of ATF6α induces transcription of UPR-related genes that promote protein folding and degradation.

Although the three major UPR systems are shown to function ubiquitously, recent studies indicate that tissue-specific UPR systems involving the ATF6α family proteins play fundamental roles in the local homeostasis. OASIS (also known as cyclic AMP response element–binding protein 3 like protein 1; Creb3l1) or BBF2H7 (Creb3l2) are important for the bone formation [6,7]. CREB4 (Creb3l4) is specifically expressed in testis and essential for the testicular spermatogenesis [8]. CREBH (Creb3l3) is also an ATF6-family member that is highly expressed in the liver and intestine [9–11]. To date, CREBH has been reported to mediate ER stress-dependent induction of acute-phase proteins in the liver, control of iron homeostasis by regulating the induction of hepcidin, and mediation of hepatic gluconeogenesis under a starvation condition [12–14].

The liver is a critical organ for detoxification of various drugs [15]. Recently, IRE1α is shown to be essential for protecting mice from hepatotoxicity of an analgesic drug acetoaminophen (APAP) [16]. XBP1-deficient mice displayed resistance to the APAP-induced fatal side effect due to feedback hepatic activation of

IRE1α, leading to degradation of mRNA of cytochrome P450 genes such as CYP1A2 and CYP2E1, those of which play critical roles in oxidation of APAP to generate a major APAP metabolite that causes the fatal side effect. In addition, c-jun N-terminal kinase, which is activated in response to ER stress, has recently been identified as a critical determinant of the APAP-induced fatality [17,18]. Thus, accumulating evidence suggests a potential link between hepatic ER stress and drug-induced fatality, however, the function of an ER stress protein CREBH that is remarkably expressed in the liver has not been studied so far in the context of drug-resistance or -susceptibility.

In this study, we show that CREBH-deficient mice are highly resistant to fatal shock induced by an antipyretic analgesic drug sulpyrine, but not by APAP. The hepatic mRNA expression of the CYP2B family members, which are important for the generation of sulpyrine metabolites, is severely reduced in CREBH-deficient mice. Moreover, ectopic expression of CREBH activates the CYP2B promoter, and sulpyrine treatment results in hepatic ER stress and nuclear translocation of CREBH. Furthermore, transient *in vivo* suppression of CREBH protects mice from sulpyrine-induced fatality. Thus, these results indicate that CREBH is critically involved in the sulpyrine-induced fatal shock by regulating hepatic expression of CYP2B family members.

## Results

### CREBH-deficiency confers mice on resistance to sulpyrine-induced shock

Because CREBH is remarkably expressed in the liver, we investigated the potential role of CREBH in detoxification by analysis of CREBH-deficient mice generated by gene targeting (Figure S1). We first analysed resistance to the pyrazolone-derived antipyretic analgesic drug sulpyrine and the non-pyrazolone antipyretic analgesic drug APAP in CREBH-deficient mice. Although high-dose acetaminophen administration resulted in comparable lethality, CREBH-deficient mice were resistant to sulpyrine (Figure 1A). Next, the antipyretic effect of sulpyrine was examined in wild-type and CREBH-deficient mice. The reduction of body temperature in sulpyrine-administrated mice was more gradual than that in wild-type mice (Figure 1B). Sulpyrine is non-enzymatically hydrolysed to 4-methylaminoantipyrine (4-MAA). Then, 4-MAA is further metabolized to 4-aminoantipyrine (4-AA) and 4-formylaminoantipyrine (4-FAA) in the liver (Figure S2) [19]. Therefore, sera were taken from sulpyrine-administrated mice just prior to the death of a number of wild-type mice, and the blood concentrations of 4-AA and 4-FAA were measured by a high-performance liquid chromatography (HPLC) assay (Figure S3). Compared with wild-type mice, sulpyrine-administrated CREBH-deficient mice exhibited lower concentrations of 4-AA and 4-FAA in their sera (Figure 1C). Given that 4-AA plays an important role in the sulpyrine-mediated antipyretic effect [20,21], the mild antipyretic effect in CREBH-deficient mice is consistent with the lower concentrations of 4-AA and 4-FAA.

### CREBH increases serum level of the sulpyrine metabolite 4-AA

To determine which metabolite of sulpyrine was responsible for fatal sulpyrine shock, we directly administrated 4-AA or 4-FAA to wild-type mice. The relationship between the administration volume of both metabolites and their concentrations in the sera was analysed, and found to be directly proportional (Figure 2A). Next, we calculated the administration volume of 4-AA and 4-FAA by their concentrations in sera from wild-type and CREBH-deficient mice administrated with 2.7 mg/g sulpyrine (Figures 1C and 2A). In wild-type mice, blood concentrations of 1150 ng/μl 4-AA and 9.3 ng/μl 4-FAA corresponded to the administration volumes of 1.16 mg/g and 0.0074 mg/g, respectively. In addition, 0.89 mg/g 4-AA and 0.0049 mg/g 4-FAA were calculated to be administrated to CREBH-deficient mice (Figure 2A). Then, wild-type mice were separately challenged with the calculated administration volumes (Figure 2B). All mice administrated with both 4-FAA concentrations survived. In contrast, although all mice administrated with 0.89 mg/g 4-AA survived, those administrated with 1.16 mg/g 4-AA succumbed. Next, we examined the survival rate of mice administrated with various concentrations of both metabolites. 4-AA required almost similar concentrations to those in mice administrated with 2.7 mg/g sulpyrine. On the other hand, the lethal dose of 4-FAA was much higher than the calculated volume (Figure 2C). Together, these data suggest that the blood concentration of 4-AA, but not 4-FAA, is well correlated with sulpyrine-induced fatal shock. Furthermore, we administrated 1.1 mg/g 4-AA, in which 60% of mice did not survive, to wild-type mice, and compared the time-dependent blood concentrations of 4-AA in the sera between surviving and dead mice. Compared with surviving mice, dead mice showed higher blood concentrations of 4-AA in their sera. Considering the survival rate of both groups, almost 1000 ng/μl 4-AA in serum was the threshold between survival and death (Figure S4A). To further investigate the difference of sensitivity to 4-AA and 4-FAA between wild-type and CREBH-deficient mice, we administrated 1.1 mg/g 4-AA and 4-FAA to wild-type and CREBH-deficient mice. Consequently, no difference was found in the sensitivity to 4-AA and 4-FAA between wild-type and CREBH-deficient mice (Figure S4B). To confirm whether CREBH deficiency conferred resistance to sulpyrine-induced fatal shock, we transfected human CREBH expression vectors into CREBH-deficient mice *in vivo*, and tested whether reintroduction of CREBH expression restored sulpyrine-induced shock in CREBH-deficient mice. Hepatic expression of hCREBH mRNA and protein was confirmed by quantitative RT-PCR and immunohistochemical assays, respectively (Figure S5A and S5B). CREBH-deficient mice with introduced hCREBH showed a significantly lower survival rate than that of control mice (Figure 1D). Accordingly, blood concentrations of 4-AA and 4-FAA in hCREBH-introduced mice were markedly higher than those in control mice. In particular, blood concentrations of 4-AA exceeded the lethal concentration threshold (Figure 1E). Collectively, these data indicate that CREBH plays an important role in modulating the 4-AA concentration in serum and fatal shock induced by sulpyrine administration.

### CREBH-deficient mice are impaired in sulpyrine-induced expression of CYP2B family genes in the liver

Because CREBH is highly expressed in the liver, we performed microarray analysis of hepatic samples from wild-type and CREBH-deficient mice to compare gene expression profiles in response to sulpyrine. Out of 22690 transcripts, we first defined genes up-regulated by more than 2.5-fold after sulpyrine administration to wild-type mice as "sulpyrine-inducible genes" and identified 423 such genes. We next compared sulpyrine-inducible genes in wild-type and CREBH-deficient mice after sulpyrine administration, and found that 105, 287 and 31 genes were down-regulated, similarly expressed and up-regulated in CREBH-deficient mice, respectively (Figure 3A and Table S1). Microarray analysis also revealed that among the down-regulated genes, expression of CYP2B family genes was severely impaired in CREBH-deficient mice. CYP2B family genes play a role in sulpyrine metabolism [22–24]. Therefore, we tested whether

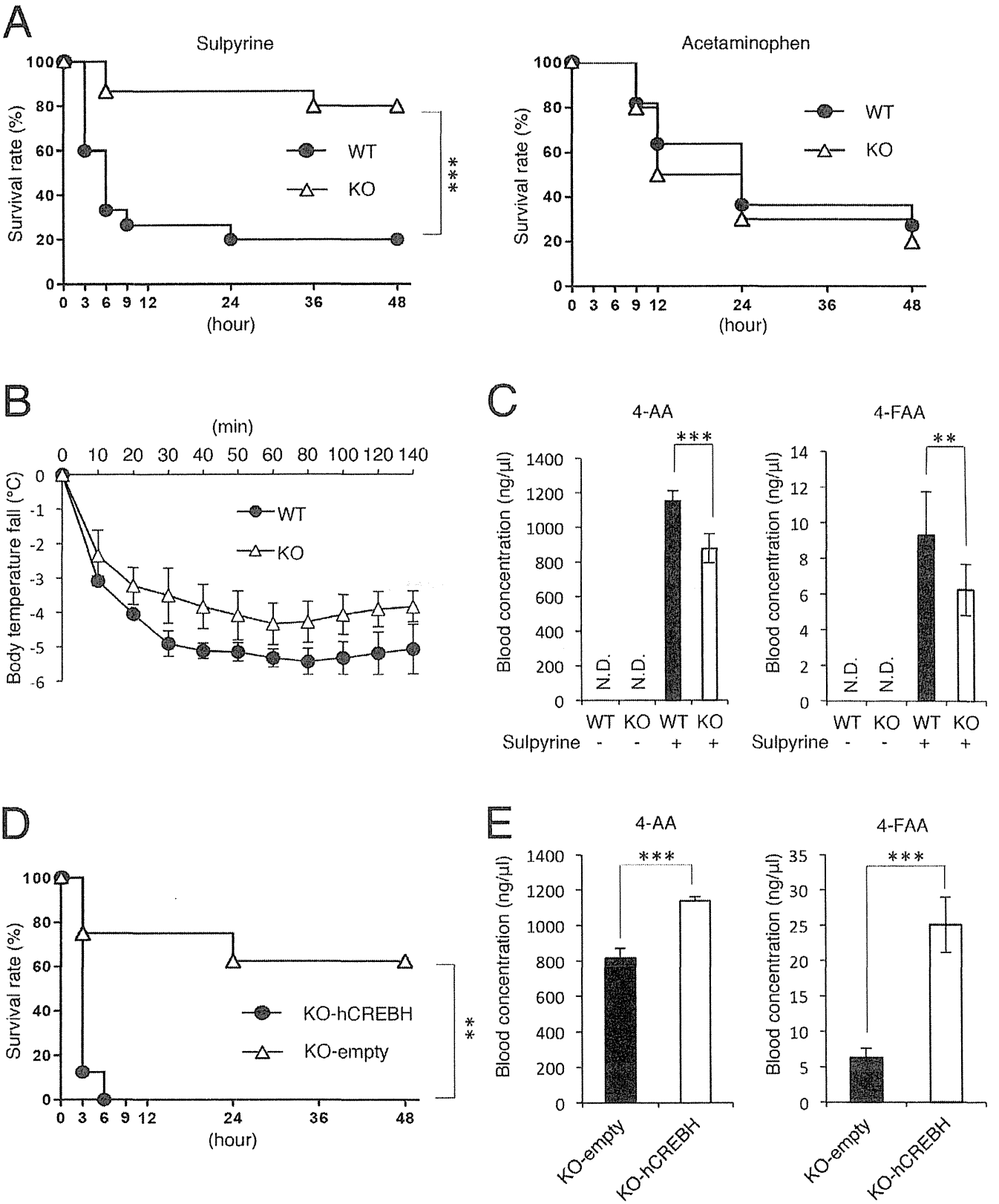


**Figure 1. CREBH-deficient mice are resistant to fatal sulpyrine shock.** (A) Wild-type (n = 15) and CREBH-deficient (n = 15) mice were intraperitoneally injected with 2.7 mg/g of sulpyrine (left). Wild-type (n = 11) and CREBH-deficient (n = 10) mice were intraperitoneally injected with 0.7 mg/g of acetaminophen (right). Survival rates were monitored for 48 hr, respectively. (B) Wild-type (n = 5) and CREBH-deficient (n = 5) mice were intraperitoneally injected with 2.7 mg/g of sulpyrine. Rectal temperature was measured at every 10 min for 140 min. (C) Wild-type (n = 10) and CREBH-deficient (n = 10) mice were intraperitoneally injected with 2.7 mg/g of sulpyrine. Sera were taken at 2 hr 40 min after sulpyrine injection.

Serum concentrations of 4-AA and 4-FAA were measured by a HPLC assay. N.D., not detected. **, P<0.01; ***, P<0.001. (D) CREBH-deficient mice transfected with hCREBH expression vectors (n = 8) or empty vectors (n = 8) were intraperitoneally injected with 2.7 mg/g of sulpyrine. Survival rate was monitored for 48 hr. (E) CREBH-deficient mice transfected with hCREBH expression vectors (n = 3) or empty vectors (n = 3) were intraperitoneally injected with 2.7 mg/g of sulpyrine. Sera were taken at 2 hr 40 min after sulpyrine injection. Serum concentrations of 4-AA and 4-FAA were measured by a HPLC assay. ***, P<0.001. Data are pooled from two (A, D) independent experiments or representative of three (C) and two (B, E) independent experiments.
doi:10.1371/journal.pone.0055800.g001

CYP2B family genes in the liver were induced in sulpyrine-administered mice by northern blot analysis. Sulpyrine administration to wild-type mice resulted in strong mRNA expression of CYP2B family genes. On the other hand, sulpyrine-induced expression was much lower in livers from sulpyrine-administrated CREBH-deficient mice (Figure 3B), whereas no difference was found in the expression of other cytochrome P450 family genes, such as CYP2A4, CYP2C37 and CYP3A25, which are not involved in sulpyrine metabolism (Figure 3C). These results suggest that sulpyrine shock in CREBH-deficient mice might be suppressed due to the low expression of CYP2B family genes. CYP2B gene has been shown to be induced by phenobarbital or dexamethasone, which activates constitutive androstane receptor (CAR) or pregnane X receptor (PXR) respectively [25–29]. We found robust induction of CYP2B family genes in the livers from CREBH-deficient mice treated with phenobarbital or dexamethasone by quantitative RT-PCR assays (Figure 3D), suggesting that CREBH is not involved in CAR-mediated or PXR-mediated induction of CYP2B family genes. Furthermore, CREBH-deficient mice pre-treated with phenobarbital were sensitive to sulpyrine (Figure 3E), indicating that hepatic expression of CYP2B genes induced by phenobarbital may confer sensitivity to sulpyrine in CREBH-deficient mice. To test this hypothesis directly, we administered a human CYP2B6 expression vector to CREBH-deficient mice *in vivo*. Quantitative RT-PCR and immunohistochemical assays confirmed hepatic expression of hCYP2B6 mRNA and protein, respectively (Figure S6A and S6B). CREBH-deficient mice with hCYP2B6 expression were more sensitive to sulpyrine than control mice (Figure 3F). Moreover, blood concentrations of 4-AA and 4-FAA in hCYP2B6-expressing mice were higher than those in control mice (Figure 3G). Together, these results demonstrated that the mechanism by which CREBH-deficient mice exhibit resistance to sulpyrine is due to the lack of sulpyrine-induced expression of CYP2B family genes in their livers.

## CREBH activates the CYP2B10 promoter

To examine whether CREBH controlled the expression of CYP2B genes, we generated a luciferase reporter plasmid harbouring the CYP2B10 promoter, and introduced the reporter plasmid into Huh7 cells together with CREBH expression vectors to measure the promoter activity by a luciferase assay. Overexpression of full-length CREBH activated the CYP2B10 promoter. In addition, promoter activation by ectopic expression of CREBH lacking the C-terminus (CREBH-ΔC), a constitutively active form of CREBH, was more enhanced than that by full-length CREBH (Figure 4A), indicating that CREBH positively regulates the expression of the CYP2B10 gene. Subsequently, to determine a CREBH responsive region in the CYP2B10 promoter, reporter plasmids harbouring various lengths of the CYP2B10 promoter were constructed, and the promoter activities were measured by a luciferase assay. Reporters containing 2650 or 1450 bp were both activated. In contrast, reporters containing 1250 bp or less were not activated, suggesting that the CREBH responsive region may be located between −1450 and −1250 bp in the CYP2B10 promoter (Figure 4B). In addition to CREBH, CAR positively regulates CYP2B10 gene expression. The CAR-responsive element, called the Nr1 region, is located at −2350 bp (Figure S7A) [30]. To analyse whether CAR was involved in CREBH-dependent activation of the CYP2B10 promoter, we compared the luciferase activities of reporters containing and lacking Nr1 in the presence of CAR or CREBH. Activation of the Nr1-containing reporter in the prescience of CAR was stronger than that lacking Nr1. Conversely, in the presence of CREBH, both reporters were similarly activated (Figure S7B). Moreover, we isolated hepatocytes from wild-type and CREBH-deficient mice by perfusion, introduced CYP2B10 promoter reporter plasmids containing Nr1 into the hepatocytes together with CAR expression vectors, and then performed a luciferase assay. CAR-induced activation of the CYP2B10 promoter was comparable between wild-type and CREBH-deficient hepatocytes (Figure S7C). These results indicated that CREBH and CAR may independently regulate hepatic expression of the CYP2B10 gene, and may be consistent with the results of phenobarbital-treated CREBH-deficient mice, in which the CYP2B gene was induced in a CAR-dependent manner, thereby conferring sensitivity to sulpyrine (Figure 3D and 3E).

## CREBH is activated by sulpyrine-induced ER stress

Previous studies have shown that CREBH is activated in an ER stress-dependent manner, and mediates the expression of genes associated with the unfolded protein response [9,12,31]. To clarify whether hepatic ER stress was induced by sulpyrine administration, we isolated hepatocytes from wild-type sulpyrine- and tunicamycin-administrated mice, and then measured the expression of CCAAT/enhancer binding protein homologous protein (CHOP) mRNA and the spliced form of X-box binding protein 1 (XBP1), indicator of ER stress, by a quantitative RT-PCR assay [12]. Sulpyrine administration similarly induced the expression of CHOP mRNA and splicing of XBP1 mRNA in response to tunicamycin (Figure 4C). To test whether CREBH was cleaved and its N-terminus was translocated into the nucleus upon stimulation with sulpyrine, we introduced CREBH expression vectors into 293T cells, and then analysed the cleavage and localization of CREBH by western blot and immunofluorescence assay, respectively. Notably, sulpyrine treatment caused the cleavage of CREBH (Figure 5A) and nuclear translocation of CREBH (Figure 5B). The extent of sulpyrine-induced nuclear localization of CREBH was similar to that by tunicamycin, while CREBH-ΔC was steadily localized in the nucleus without stimulation (Figure 5C). Taken together, these results indicate that sulpyrine administration possibly induces ER stress in the liver and results in activation of CREBH, leading to expression of the CYP2B10 gene.

## The CREBH-knockdown mice exhibit resistance to fatal sulpyrine shock

Despite the strong antipyretic effect, fatal shock induced by sulpyrine is so clinically problematic that use of this drug is restricted and even prohibited in several countries [32]. Therefore, fatality should be precluded in advance for the safe usage of sulpyrine. We attempted to prevent sulpyrine shock by transient reduction of CREBH in wild-type mice. First, we selected an efficient RNAi vector against CREBH *in vitro* (Figure S8),